BNL-108524-2015-IR

eRHIC/46
October 2015

Report of the eRHIC Ring-Ring Working Group

**E.C. Aschenauer, S. Berg, M. Blaskiewicz,
M. Brennan, A. Fedotov, W. Fischer, V. Litvinenko,
C. Montag, R. Palmer, B. Parker, S. Peggs, V. Ptitsyn,
V. Ranjbar, S. Tepikian, D. Trbojevic, F. Willeke**

**Collider-Accelerator Department
Brookhaven National Laboratory
Upton, NY 11973**

**U.S. Department of Energy
Office of Science, Office of Nuclear Physics**

Report of the eRHIC Ring-Ring Working Group

F C Antoniazzi, S Berg, M Blaskiewicz, M Bruker, A Fedotov, W Fischer, V Litvinenko, C Montag (chair), R Palmer, H Path, S Peggs, V Ptitsyn, V Ranjbar, S Tepikian, D Trbojevic, F Willeke

eRHIC-46
October 14, 2013

Acknowledgements

We are very pleased to acknowledge the support, advice and wisdom of I. Ben-Zvi, M. Harrison, G. Hoffstaetter, J. Kewisch, T. Roser, and Y. Zhang. Their intellectual contributions were vital in the construction of this report.

Report of the eRHIC Ring-Ring Working Group
C-A/eRHIC/46
October 13, 2015

Contents

List of Figures

List of Tables

Executive Summary

This report evaluates the ring-ring option for eRHIC as a lower risk alternative to the linac-ring option. The reduced risk goes along with a reduced initial luminosity performance. However, a luminosity upgrade path is kept open.

This upgrade path consists of two branches, with the ultimate upgrade being either a ring-ring or a linac-ring scheme. The linac-ring upgrade could be almost identical to the proposed linac-ring scheme, which is based on an ERL in the RHIC tunnel. This linac-ring version has been studied in great detail over the past ten years, and its significant risks are known. On the other hand, no detailed work on an ultimate performance ring-ring scenario has been performed yet, other than the development of a consistent parameter set. Pursuing the ring-ring upgrade path introduces high risks and requires significant design work that is beyond the scope of this report.

The baseline ring-ring design outlined in this report has the following advantages:

1. It is based almost completely on existing technologies. This reduction of technical risk can speed up the process for launching an eRHIC construction project.
2. Less budget contingency is required, reducing the Total Project Cost.
3. Easier commissioning and ramp up. Less time and effort is expected to reach an operational level of facility performance, enabling the science program to start earlier.

The Ring-Ring Working Group evaluated four charge questions listed below, for ring-ring configurations that cover the entire center-of-mass energy range, with polarized electrons up to 20 GeV colliding with either 250 GeV polarized protons, or 100 GeV/nucleon gold ions. Sufficient detector acceptance for the physics case was included for a **baseline** configuration, and was assumed for luminosity staging **upgrade levels** 1 and 2. The predicted e+p luminosity performance is shown in Table 1 and Figure 1. Further, it was assumed that:

1. The eRHIC electron storage ring is in the existing RHIC tunnel.
2. There is initially only one detector with one collision per turn.
3. Baseline hadron beam parameters only modestly exceed those already demonstrated in RHIC, except that the number of bunches is increased from 120 to 360 (before considering the abort gap).
4. The electron storage ring has a full energy injector.
5. The maximum electron beam-beam parameter is given by $\xi_{e,max} = 1.37\ \delta^{1/3}$, where δ is the transverse damping decrement, as demonstrated by KEKB.
6. The maximum linear synchrotron radiation load is 10 kW/m in the arcs, leading to a total power of up to 24 MW.

Little time was available to develop the ring-ring design that is presented in this report, which is not backed up by detailed calculations and simulations, or by detailed technical layouts and designs. Report conclusions are deduced from experience with existing facilities, from conventional wisdom, and

Parameter		**e+p**
Center-of-mass energy $\sqrt{s}$	GeV	32 – 141
Electron energy	GeV	5 – 20
Hadron energy	GeV	50 – 250
Baseline maximum luminosity	$10^{33}\text{cm}^{-2}\text{s}^{-1}$	2.0
Upgrade 1 maximum luminosity	$10^{33}\text{cm}^{-2}\text{s}^{-1}$	4.7
Upgrade 2 maximum luminosity	$10^{33}\text{cm}^{-2}\text{s}^{-1}$	12.7
Transverse electron polarization	%	≥ 75
Hadron (p,h) polarization	%	70
Number of bunches		360 – 6000
Bunch spacing	ns	35 – 2

Table 1: Baseline and upgrade level 1 and 2 scenarios. Luminosity versus energy is shown in Figure 1. The e+p luminosity is approximately the same as the e+nucleon luminosity for collisions with heavy ions.

using scaling laws. Naturally there are a number of questions that deserve more work and investigation, especially on the upgraded ring-ring stages. This is beyond the scope of this working group report.

This preliminary study is sufficiently adequate and reliable to answer the charge questions below. The remaining open questions can be satisfactorily resolved by investing more time and effort to further develop the ring-ring design. Open items that require further study are pointed out in the body of the text after this Executive Summary, so that that reader can better judge whether the conclusions drawn here are accurate.

1. Can the EIC physics goals be achieved with a ring-ring eRHIC option?

Yes, for three out of the four areas that we evaluated: (i) energy range, (ii) proton, helium and electron spin polarization, and (iii) detector requirements. Yes with qualifications, for the fourth area: (iv) luminosity.

(i) *Energy range.* See Section 4.1. An energy change requires a path length adjustment of up to 65 cm to account for the change in the speed of the hadrons. This adjustment is made in a combination of three methods: chicanes in the electron ring that are also used to enhance synchrotron radiation damping at lower energies; using different inner and outer arcs of the hadron ring; and having a radial offset in the hadron ring.

(ii) *Spin polarization.* See Section 4.2. Proton polarizations of up to 60% have been demonstrated in RHIC using two Siberian snakes (per ring). Six Siberian snakes will be required to preserve the polarization of helium-3 beam in eRHIC. This increased number of snakes will help to achieve 70% polarization of protons. The helical magnets in the snakes and spin rotators could be used to built four more Siberian snakes. Rotators provide transverse or longitudinal proton spin at the experiment. R&D work on a polarized helium-3 source for eRHIC is ongoing. Transverse electron polarization levels exceeding 75% have been achieved in several storage rings operating above 10 GeV. High polarization levels in eRHIC demand the full energy injection of pre-polarized electrons into the storage ring. Electron spin rotators appear to be feasible over the full energy range, using a combination of solenoids and skew quadrupoles. The longitudinal spin projection varies between 0.85 and 1 over the energy range.

(iii) *Detector requirements.* See Section 3.1. A nominal interaction region layout has ± 4.5 m of free space around the interaction point available for a central detector, and 2 m of free space available for

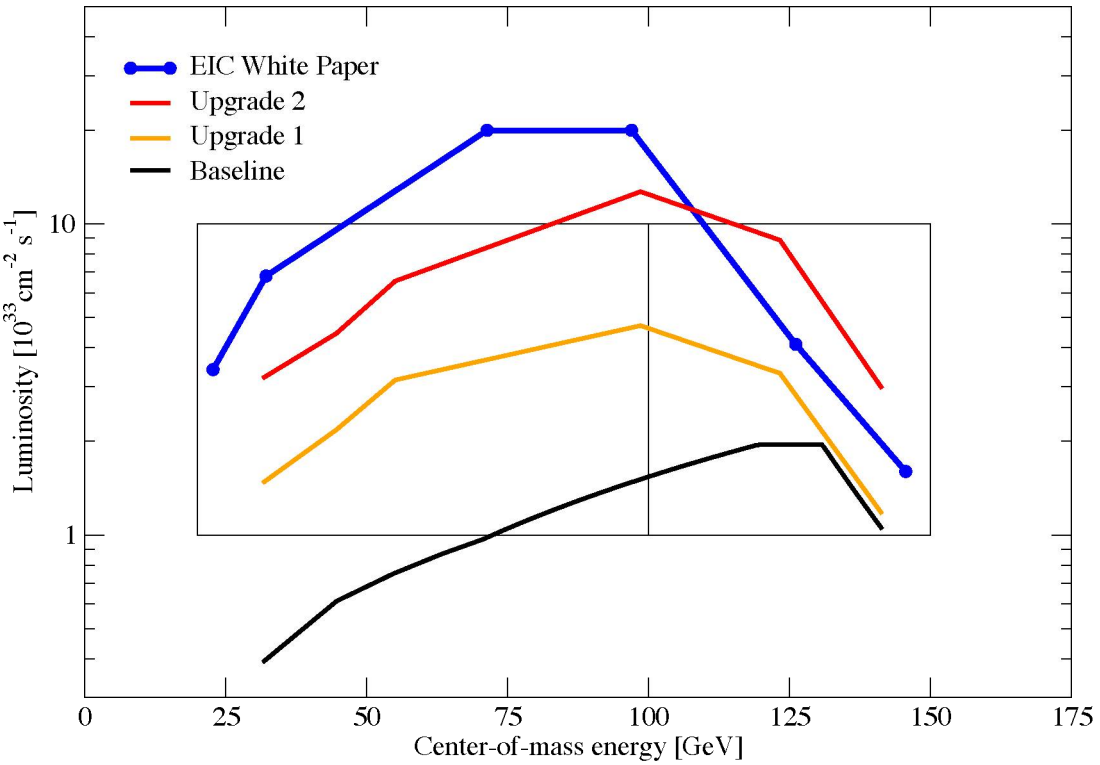

Figure 1: Luminosity versus center-of-mass energy in baseline and upgrade scenarios. Upgrade level 1 requires some electron cooling at all energies to reduce the proton and ion emittances. Upgrade level 2 requires order-of-magnitude emittance reductions, perhaps only possible with Coherent Electron Cooling.

Roman Pots between the dipoles of the dogleg that bends the proton beam in the horizontal plane, with 10 sigma beam divergence. A 4 mrad opening cone is preserved for neutron detection, with a full crossing angle of 15 mrad between proton and electron beams, requiring crab cavities to restore luminosity. Spin patterns containing bunches of opposite polarization can be used, thanks to the long self-polarization time, and the pre-polarized injected beam. Beam-gas background rates appear to be acceptable, even for the 2 ns bunch spacing in upgrade level 2.

(iv) *Luminosity.* See Section 2.1, Table 1, and Figure 1. Some longitudinal cooling is required in the baseline scenario at the lowest energies, to maintain the proton bunch length. Assuming technical solutions for a ring-ring upgrade scheme can be found, Upgrade level 1 increases the luminosity by approximately a factor of 4 except at the highest energies. This requires electron cooling at all energies to reduce the proton and ion emittances, both transverse and longitudinal, by factors of approximately 2.5. Upgrade level 2 increases the luminosity by an order of magnitude or more over the whole energy range, requiring emittance reductions closer to one order of magnitude, perhaps only possible with Coherent Electron Cooling. If a linac-ring scheme is chosen as the upgrade path, luminosities that are generally comparable with the ring-ring upgrade stage 2 or with luminosities stated in the EIC White Paper for the linac-ring version can be achieved, as shown in Figure 1.

2. Can the MEIC design (high bunch repetition rate and low bunch charge, but without figure-8) be adapted for use with eRHIC and if not why not?

Yes, high repetition rates of low intensity bunches can be adapted for use with eRHIC. See Section 2.1. The MEIC design is similar in beam parameters to upgrade level 2, with 2 ns bunch spacing. The basic

ideas used in the study of upgrades with many bunches have been discussed before, for example by Ben-Zvi et al [1] and Zhang [3], although the constraints used here, and the resulting parameters, are different. Upgrades 1 and 2 require additional cooling.

3. What are the risks of a ring-ring option?

The two leading risks in the baseline configuration are (i) crab cavities, and (ii) electron cooling of hadrons. More aggressive cooling and an interaction region design with β-functions below 10 cm are additional risks in upgrade configurations 1 and 2.

(i) *Crab cavities.* See Section 5.1. Crab cavities have been operated in the e^+e^- collider KEKB, and are part of the HL-LHC upgrade. The eRHIC crab cavities in the baseline configuration, which have a frequency of 168 MHz and a total voltage of 7.4 MV, can be normal or superconducting. As in the LHC, beam-beam dynamics, low-noise operation, and machine protection issues need to be addressed. Additional harmonic crab cavities may be needed, due to the significant RF curvature, but these would not introduce an additional risk. An interaction region with a dipole field in the detector instead of crab cavities is conceivable, but the design would be challenging.

(ii) *Electron cooling of hadrons.* See Section 5.2. Some longitudinal cooling is required in the baseline scenario at the lowest energies, to maintain the proton bunch length. Electron cooling is required at all energies, to upgrade the luminosity from the initial values. Upgrade level 1 requires magnetized cooling to reduce the proton and ion emittances, both transverse and longitudinal, by factors of the order of 2.5. The required beam and solenoid parameters go beyond current experience, although the physics of magnetized cooling is well established. Upgrade level 2 assumes emittance reductions closer to one order of magnitude. This requires a new technique, and is perhaps only possible with Coherent Electron Cooling.

4. Is there a possibility to start with ring-ring and then upgrade to linac-ring?

Yes. See Section 2.2. The ring-ring version of eRHIC could be converted to a linac-ring design using an electron ERL. In this case many high-risk items installed gradually during the ring-ring upgrade process would still be used, such as the (Coherent) Electron Cooler and the crab cavity system. The electron ring with its spin manipulating devices (spin rotators) would be used as a separate loop for the highest energy beam in the ERL. The detector would remain in place, as would the arrangements for hadron path length adjustment.

An electron injector based on a recirculating linac using superconducting RF technology could provide a natural upgrade path towards a linac-ring eRHIC.

Chapter 1

Introduction

1.1 Charge to the working group

Thomas Roser wrote to Christoph Montag (May 22, 2015):

> "Now that it is likely that the EIC will be recommended as the next facility construction after FRIB we have an opportunity to critically review and reassess the eRHIC design and plan a focused and credible R&D program. As part of this I would like to ask you to take a second look at the ring-ring option for eRHIC.
>
> Our approach to eRHIC has been and should continue to be:
>
> 1. The initial configuration of eRHIC should have enough center-of-mass reach (20 GeV polarized electrons colliding with 250 GeV polarized protons, and 20 GeV electrons colliding with 100 GeV/n gold ions), and enough detector acceptance, to cover the whole EIC physics case.
> 2. The initial luminosity could be lower and then be increased through incremental upgrades, as was done for RHIC.
>
> Please address these questions:
>
> 1. Can the EIC physics goals be achieved with a ring-ring eRHIC option following the above approach?
> 2. Can the MEIC design (high bunch repetition rate and low bunch charge, but without figure-8) be adapted [for] use [with] RHIC and if not why not?
> 3. What are the risks of a ring-ring option?
> 4. Is there a possibility to start with ring-ring and then upgrade to linac-ring?
>
> Please prepare a report that answers these questions in about three months. Much of the work can use information from the earlier ring-ring eRHIC design report."

Question 1 – **achieving physics goals** – see Sections 2.1, 3.1, 4.1, and 4.2.
Question 2 – **many low charge bunches** – see Section 2.1: for example Figure 2.1 and Table 2.2.
Question 3 – **ring-ring risks** – see Chapter 5.
Question 4 – **upgradability to linac-ring** – see Section 2.2.

1.2 Assumptions and ground rules

A number of assumptions and ground rules limited the scope of this working group report, within the relatively short amount of time available to answer the charge questions. This is *not* a Design Report. Costs have not been considered, parameters have not been optimized, and not all issues have been identified or addressed. Nonetheless, a list of leading issues that qualify the answers to the charge questions has been identified. These issues need further study, if the evaluation of the ring-ring option is to proceed.

Basic assumptions

The luminosities quoted in this report are normalized to assume that eRHIC operates with one collision per turn at one interaction point. This does not preclude the possibility of operating with two detectors, an upgrade that is preserved. Both detectors will not necessarily work at the same time.

Only electron-proton and electron-gold collisions are considered, although collisions with other ion species are possible. A positron upgrade is not ruled out.

Interaction region design assumptions are discussed in Sections 3.1 and 3.2, and in reference [4].

RF frequency and bunch spacing are free parameters, even though a fundamental frequency of 28 MHz (equivalent to 360 bunches) is implicitly assumed in some cases.

A full energy electron injector delivers pre-polarized beams. Three injector options are presented in Section 2.3: a section of the SLAC linac as suggested by Zhang [3]; a figure-of-8 synchrotron similar to the MEIC storage ring; and a recirculating linac.

Hadron performance parameters of current RHIC beams are assumed in general, except where explicitly stated otherwise (with some minor plausible exceptions).

The electron energy E_e drops more quickly than E_{ion} as the center-of-mass energy

$$E_{COM} \;=\; 2\sqrt{E_e E_{ion}} \tag{1.1}$$

decreases, enabling the synchrotron radiation load to be reduced (in some scenarios).

Beam-beam intensity limits

The maximum electron beam-beam tune shift parameter (caused by ions) is

$$\xi_{e,max} \;=\; 1.37\;\delta^{1/3} \tag{1.2}$$

based on KEKB experience ($\xi = 0.08$ with $\delta = 2 \times 10^{-4}$ [5]). The damping decrement δ is the fraction of a transverse damping time that occurs between beam-beam collisions, with a natural value

$$\delta \;=\; \frac{U_0}{2\,E_e} \tag{1.3}$$

where U_0 is the energy radiated by an electron on very turn, when the partition number is not deliberately modified and there is one collision per turn. Section 4.1 discusses how wigglers can be used to increase δ at lower electron energies, thereby also increasing $\xi_{e,max}$.

The maximum ion beam-beam parameter (caused by electrons) is assumed to be $\xi_{p,max} = 0.015$.

Synchrotron radiation

In one turn of a storage ring with bending magnets of radius ρ, an electron of energy E_e loses

$$U_0\ [\mathrm{MeV}] \;=\; 0.0885\;\frac{E_e^4\ [\mathrm{GeV}^4]}{\rho\ [\mathrm{m}]} \tag{1.4}$$

and the total power radiated by a circulating electron current I_e is given by

$$P\ [\mathrm{MW}] \;=\; U_0\ [\mathrm{MeV}]\ I_e\ [\mathrm{A}] \tag{1.5}$$

showing that the synchrotron radiation power decreases rapidly as the energy decreases [6].

The synchrotron radiation damping time is

$$\tau_i \text{ [ms]} = \frac{C \text{ [m]} \, \rho \text{ [m]}}{13.2 \, J_i E^3 \text{ [GeV}^3\text{]}} \tag{1.6}$$

Natural values $(J_H, J_V, J_S) = (1, 1, 2)$ are assumed for the horizontal, vertical, and longitudinal damping partition parameters, although some performance advantages may be available from their optimization.

The critical photon energy is

$$\varepsilon_c \text{ [keV]} = 2.22 \, \frac{E^3 \text{ [GeV}^3\text{]}}{\rho \text{ [m]}} \tag{1.7}$$

The practical engineering limit for the linear power load, $P/2\pi\rho$, is taken to be $P_{lin,max} = 10$ kW/m, averaged over the entire cell (or arc) length, not just over the dipoles. A small number of special exceptions may be made.

The maximum installed RF power – around 24 MW – is calculated from the linear load limit. Full installation of RF is assumed for simplicity in the baseline scenario, although the staged installation of RF power (from a modest beginning to this maximum) is more likely in practice.

Electron storage ring

The electron storage ring is in the RHIC tunnel, using conventional electromagnets in a separated function design, operating near the half-integer tune for beam-beam resilience. The RHIC yellow ring is inactive, but is only partially removed, as necessary.

Triplet Bend Achromat and FODO arc cell optics are compared in Appendix B, evaluating the flexibility that they offer in tuning the electron emittance.

The effective FODO cell length can be doubled by turning off quadrupoles $N + 1$ and $N + 3$, and inverting the polarity of quadrupole $N + 2$ relative to N, for every FODO macro-cell.

Super-bend optics with segmented arc dipoles offer independent control of damping-decrement and emittance. This is discussed along with electron path length adjustment (necessary when the hadron energy and speed change) in Section 4.1.

Minimum energy values are $(E_e, E_p) = (5, 50)$ [GeV] and $(E_e, E_{Au}) = (5, 50)$ [GeV, GeV/u] for electron-proton and electron-gold collisions, respectively.

Interaction region geometries

Electron and hadron beams have identical rms beam sizes at the interaction point, although the horizontal and vertical beam sizes may differ.

The rms electron bunch length is very much shorter than $\sigma_{ion,s}$.

The baseline ring-ring scenario assumes that crab cavities are used to restore the luminosity lost when significant crossing angles are used to suppress parasitic long-range beam-beam collisions. Preliminary estimates by suggest that (for example) 8 MV of transverse voltage is necessary at a frequency of 168 MHz in order to restore 75% of the luminosity with a full crossing angle of 10 mrad. The RF wavelength of 1.7 m handles a hadron bunch with an rms length of $\sigma_{ion} = 0.20$ m.

Crab cavities could be eliminated, and head-on collisions re-established, if it were possible to include an appropriate dipole field in the detector. This solution seems unlikely, even though it could have significant advantages.

Cooling to combat Intra-Beam Scattering

Beam growth due to Intra Beam Scattering is not significant for the baseline parameters with protons at 160 GeV and 250 GeV, and so the proton beam does not need to be cooled at these energies. Proton cooling is required at 50 GeV, to preserve the proton bunch length at the value of $\sigma_{p,s} = 0.2$ m that is

quoted in Table 2.2. Appropriate cooling times could be obtained with a high-energy magnetized electron cooler. More details are given in Section 4.3

Currently the 95% longitudinal emittance of protons at RHIC injection is about 0.6 eV-s. At 250 GeV with an RF voltage of 4.4 MV at 197 MHz RF this corresponds to an rms bunch length of $\sigma_s = 0.2$ m, and an rms momentum spread of $\sigma_p/p = 6.5 \times 10^{-4}$. The corresponding IBS growth times for bunches with 3×10^{11} protons are $\tau_x = \tau_y = 10$ hours, and the IBS growth time of the longitudinal emittance is $\tau_z = 13$ hours.

For protons at 160 GeV, a longitudinal emittance of 0.6 eV-s and an rms bunch length of $\sigma_s = 0.2$ m should be attainable from the RHIC injectors, or by pre-cooling at RHIC injection energy. The resulting IBS growth times of the horizontal and vertical beam emittances are $\tau_x = \tau_y = 4$ hours, and the IBS growth time of the longitudinal emittance is $\tau_z = 5$ hours.

For protons at 50 GeV, longitudinal emittances that are significantly smaller than those yet achieved for high-intensity beams are required in order to get an rms bunch length of $\sigma_s = 0.2$ m. The 50 GeV IBS calculation in Table 2.2 assumes that a longitudinal emittance of 0.3 eV-s can be obtained by pre-cooling at the RHIC injection energy, or by cooling directly at 50 GeV. The resulting IBS growth times of the horizontal and vertical beam emittances are $\tau_x = \tau_y = 0.5$ hours, and the IBS growth time of the longitudinal emittance is $\tau_z = 0.6$ hours.

Polarization

The natural polarization time due to the Sokolov-Ternov effect, in an isomagnetic ring with $C = 3,833$ m, and $\rho = 300$ m, is

$$T_{\rm pol}\ [\rm s] \ = \ \frac{99\, C\rho^2}{2\pi (E_e[\rm GeV])^5} \tag{1.8}$$

So, the fastest and slowest self-polarization times are about 1,700 seconds and 1.74×10^6 seconds when $E_e = 20$ GeV and 5 GeV, respectively. While it may be possible to rely on self-polarization at energies above (say) 15 GeV – in HERA the time to equilibrium polarization was about 20 minutes – clearly the injector must deliver pre-polarized beam to the electron storage ring at least in the range from 5 GeV to 15 GeV.

Luminosity, beam-sizes, and emittances

The luminosity is

$$L \ = \ F_{\rm rev}\, \frac{M N_e N_i}{4\pi \sigma_H^* \sigma_V^*} \tag{1.9}$$

where σ_H^* and σ_V^* are the horizontal and vertical beam sizes, M is the number of bunches in each beam, and N_e and N_i are the single bunch populations for electrons and ions. The rms ion and electron beam sizes at the interaction point are

$$\begin{aligned} \sigma_i^* &= \sqrt{\frac{\beta_i^* \epsilon_i}{\beta \gamma_i}} \\ \sigma_e^* &= \sqrt{\beta_e^* \epsilon_e} \end{aligned} \tag{1.10}$$

where ϵ_i is the rms *normalized* ion emittance, and the electron emittance ϵ_e is *unnormalized*. The *unnormalized* electron and ion emittances scale in opposite directions with energy, as

$$\begin{aligned} \epsilon_{U,i} &\propto \gamma_i^{-1} \\ \epsilon_e &\propto \gamma_e^2 \end{aligned} \tag{1.11}$$

due to adiabatic damping and synchrotron radiation damping, respectively.

Fixed primary parameters

The assumed numerical values of some fixed primary parameters are shown in Table 1.1, in addition to the other assumptions described in the text.

Parameter		**Value**
Linear synchrotron radiation load (max)	kW/m	10
Proton bunch intensity (max) N_p		3×10^{11}
Gold bunch intensity (max) N_{Au}		2×10^9
Gold and proton beam-beam parameter (max) ξ_i		0.015
Electron ring circumference, C	m	3833
Electron arc dipole bend radius, ρ_D	m	300.6
Electron arc average radius, ρ_{tunnel}	m	380.5
Proton beam emittance (rms, normalized), ϵ_p	μm	2.5
Gold beam emittance (no cooling), ϵ_{Au}	μm	2.5

Table 1.1: Fixed numerical assumptions.

Chapter 2

Luminosity, upgrades, and options

2.1 Luminosity

The baseline scenario assumes beam parameters similar to those already achieved in RHIC, with some modest extrapolations. For instance, proton bunch intensities of up to 3×10^{11} protons per bunch are assumed in the design, a 25 percent increase over the 2.4×10^{11} routinely achieved in the recent run. Normalized rms emittances of $\epsilon_N = 2.5$ μm are routinely achieved, and are assumed. The existing 28 MHz RF system can store the 360 bunches in the baseline – three times as many as the current maximum of 120 (ignoring abort gaps). – although a faster injection kicker system is required. Resistive wall losses and the associated heating of the cold beampipes are issues, as also is the heating of the Beam Position Monitor (BPM) cables. Beam pipe heating can be overcome to some extent by providing more cooling power from the existing RHIC cryogenic plant. BPM cables inside the cryostats all need to be replaced.

Upgrade level		**0**	**1**	**2**
Maximum number of bunches		360	2000	6000
Maximum luminosity	$10^{33}\text{cm}^{-2}s^{-1}$	2.0	4.7	12.7
Minimum electron unnormalized H emittance	nm	53	24	11
Transverse proton rms normalized emittance	μm	2.5	0.99	0.34
Proton bunch length	cm	20	8	3.5
Crossing angle	mrad	15	22	22

Table 2.1: Parameters summarizing the baseline and upgrade level 1 and 2 scenarios.

The upgraded luminosity scenarios require a simultaneous increase in the number of bunches, a reduction of the electron charge per bunch, a reduction of emittances, and a reduction of the β-functions at the interaction point. Many of the ideas used in the study of upgrades with many bunches have been discussed before, for example by Ben-Zvi et al [1], in the eRHIC Zeroth-Order Design Report [2] and recently by Zhang [3]. However, the constraints used here, and the resulting parameters, are different. A computer aided search was undertaken to find parameters giving significant improvements in proton-electron luminosity. Two stages of upgrade are considered, with the parameters summarized in Table 2.1.

Upgrade level 1, with as many as 2,000 bunches, requires only magnetized cooling to reduce the proton and ion emittances, both transverse and longitudinal, by factors of the order of 2.5.

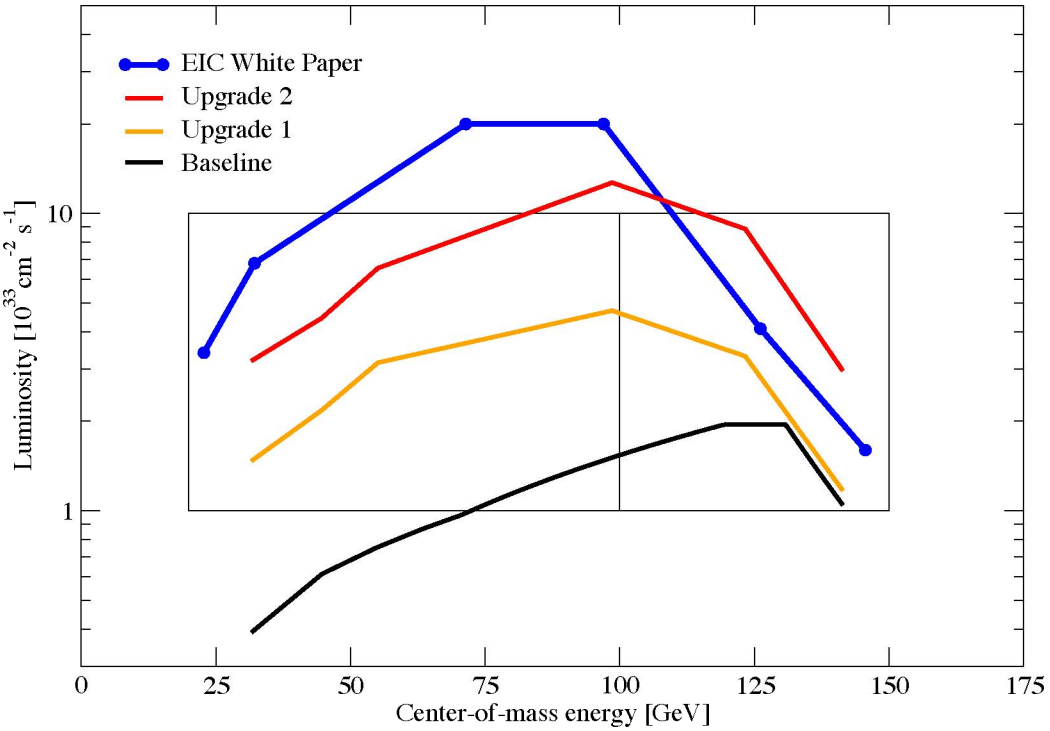

Figure 2.1: Luminosity versus center-of-mass energy in the linac-ring EIC White Paper, and in the ring-ring baseline and upgrade scenarios. Upgrade level 1 requires some electron cooling at all energies to reduce the proton and ion emittances. Upgrade level 2 requires order-of-magnitude emittance reductions, perhaps only possible with Coherent Electron Cooling.

Upgrade level 2, with as many as 6,000 bunches, assumes emittance reductions closer to one order of magnitude. This might only be possible with Coherent Electron Cooling, and requires β^* values lower than have so far been achieved for hadrons. Chromatic aberrations and dynamic aperture need to be studied.

Table 2.1 and Figure 2.1 summarize the accelerator parameters, and predict the e+p luminosity performance. Table 2.2 presents a more detailed list of baseline and upgrade Level 2 accelerator parameters. Figure 2.2 gives more details of the expected baseline luminosity performance.

2.2 Upgrading from ring-ring to linac-ring

For ultimate luminosity performance the ring-ring version of eRHIC could be converted to a linac-ring design. In this case many high-risk items installed gradually during the upgrade process of the ring-ring version would still be used, such as the (coherent) electron cooler, the crab cavity system, and the in-situ copper coated RHIC beampipes. The electron ring with its spin manipulating devices (spin rotators) would be used as a separate loop for the highest energy beam in the linac-ring configuration, eliminating the need for spin manipulation at low energy. The detector would remain in place, as would the arrangement of the various RHIC arcs for circumference adjustment, should this solution have been implemented for ring-ring operation.

On the other hand, conversion to linac-ring would make several major systems obsolete. Among these are the full energy polarized electron injector complex (unless a CEBAF-type recirculating linac is chosen for ring-ring), the electron ring RF system, and the interaction region magnets. However, in light of the large luminosity gain expected from this conversion, the evolution from ring-ring to linac-ring may still be worthwhile.

		Baseline			**Upgrade level 2**		
COM energy, E_{COM}	GeV	31.6	89.4	141.4	31.6	98.6	141.4
Luminosity, L	$10^{33}\text{cm}^{-2}\text{s}^{-1}$	.37	.42	1.06	3.2	12.7	3.0
Number of bunches, M		360	360	360	4808	5591	5591
Beam size, σ^*_H, σ^*_V	mm	.31, .110	.22, .081	.14, .051	.016, .016	.016, .008	.016, .008
ELECTRON							
Energy, E_e	GeV	5	20	20	5	11.7	20
Bunch population, N_e	10^{11}	2.08	1.14	1.14	.42	.31	.07
Beam current, I_e	A	.925	.508	.508	2.50	2.18	0.50
Energy loss per turn, U_0	MeV	.18	47.1	47.1	.18	5.4	47.1
Linear power load, P_{lin}	kW/m	.071	10.0	10.0	4.0	5.0	9.9
Arc SR power, P_{arc}	MW	.2	23.9	23.9	0.5	12.0	23.6
Wiggler SR power, P_{wig}	MW	23.7	.0	.0	9.1	.0	.0
Total SR power, P_{tot}	MW	23.9	23.9	23.9	9.6	12.0	23.6
Un. emits., $\epsilon_{eUH}, \epsilon_{eUV}$	nm	106., 19.	62.2, 11.2	53., 9.5	11.0, 2.0	10.9, 2.0	10.8, 1.9
IP betas, $\beta^*_{eH}, \beta^*_{eV}$	m	.86, .60	.61, .42	.38, .27	.023, .127	.023, .032	.023, .032
Beam diverge., $\sigma'^*_{eH}, \sigma'^*_{eV}$	mrad	.37, .19	.37, .19	.37, .19	.69, .12	.69, .25	.68, .25
B-B paras., ξ_{eH}, ξ_{eV}		.091, .178	.032, .059	.048, .096	.018, .099	.024, .066	.014, .039
Bunch length, σ_{es}	m	.012	.012	.012	.012	.012	.012
PROTON							
Energy, E_p	GeV	50	100	250	50	208	250
Bunch population, N_p	10^{11}	3.0	3.0	3.0	.09	.20	.20
N. emit., $\epsilon_p N$	μm	2.5	2.5	2.5	.34	.34	.34
IP betas, $\beta^*_{pH}, \beta^*_{pV}$	m	2.16, .27	2.16, .27	2.16, .27	.040, .040	.164, .041	.198, .049
Beam diverge., $\sigma'^*_{pH}, \sigma'^*_{pV}$	mrad	.15, .42	.105, .30	.066, .19	.40, .40	.10, .19	.08, .16
B-B paras., ξ_{pH}, ξ_{pV}		.015, .005	.008, .003	.008, .003	.015, .015	.015, .007	.003, .002
Bunch length, σ_{es}	m	.20	.20	.20	.04	.035	.035

Table 2.2: Beam and predicted electron-proton performance parameters in baseline and upgrade scenarios.

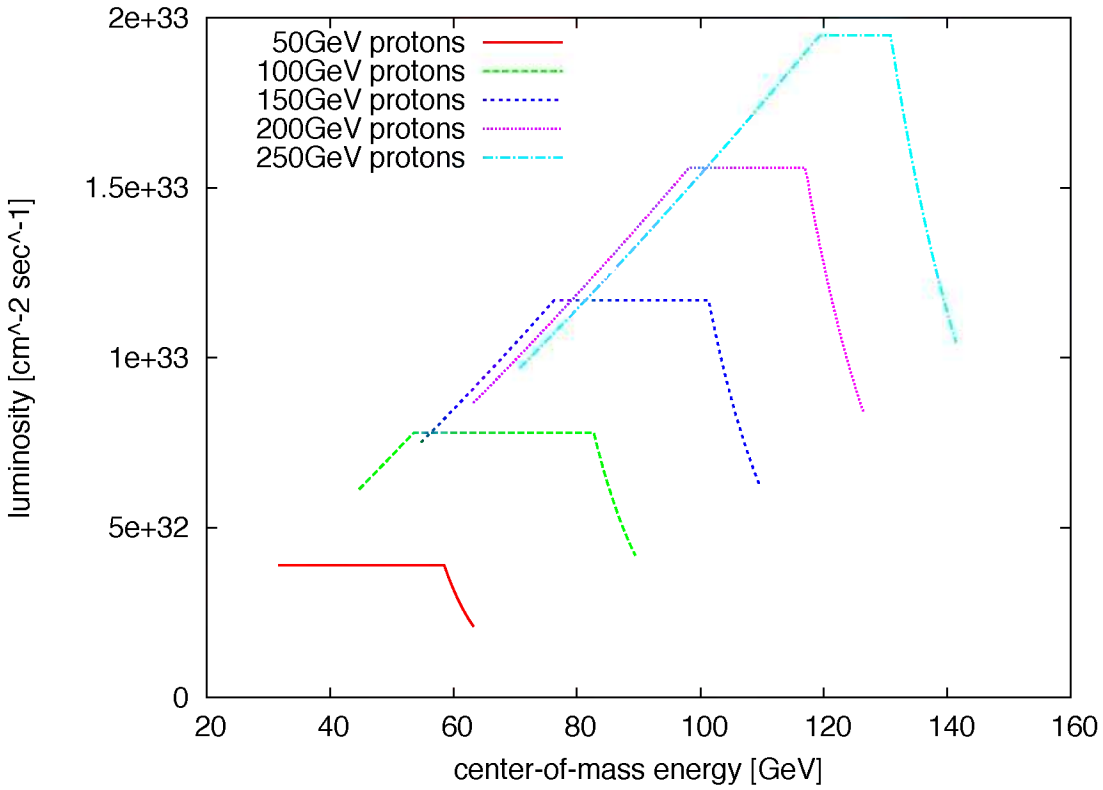

Figure 2.2: Luminosity versus c-o-m energy in the baseline scenario, for different fixed proton energies.

2.3 Injector options

The electron injector chain must allow for arbitrary spin bunch patterns in the storage ring. The Sokolov-Turnov time can be as short as 30 minutes, and large polarization is needed, so it is necessary to replace bunches at frequent intervals. We assume that it is possible to extract some bunches completely, while leaving the others alone. It is not yet clear whether it is necessary to inject full intensity bunches into the storage ring – options with multi-turn injection and full intensity single-turn injection are being considered. The same fast kicker used to extract old unpolarized bunches could be used to inject new, full intensity, fully polarized bunches.

Figure 2.3 shows a block diagram of the injector chain, with a linac, pre-injector and accumulator capable of preparing full intensity pre-polarized small emittance electron bunches for acceleration. Three options are considered for the final acceleration step: a SLAC linac section; a figure-of-8 synchrotron; and a recirculating linac.

2.3.1 Pre-injector and accumulator

The pre-injector could be a prototype within a modified scope of the Cβ project proposed jointly by Cornell University and BNL [7], as sketched in Figure 2.4. Existing polarized guns yield no more than about 1 nC per pulse, so for full intensity injection it is necessary to merge (and damp) as many as 50 individual bunches in the accumulator, before accelerating to full energy for injection into the electron storage ring.

The project uses a DC gun and injector to deliver 6 MeV electrons to a 61 MeV superconducting linac cryomodule. The 6 MeV beam stop that follows has already been commissioned at Cornell, along with the DC gun and cryomodule. Configured as an Electron Recovery Linac, the electron beam passes through the linac a total of 8 times, with energies of 67, 128, 189, and 250 MeV in both accelerating and decelerating

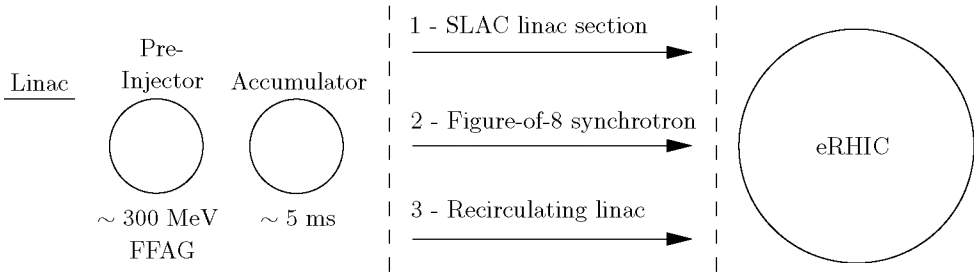

Figure 2.3: Block diagram of the injector chain, with three options for the final accelerator stage.

(energy recovery) passes. Deceleration occurs on the negative part of the sinusoidal RF voltage, after a $\pi/2$ phase shift achieved by adjusting the time of flight (path length). The return arcs in the racetrack use Fixed Field Alternating Gradient (FFAG) permanent magnet optics. On each turn beam is matched from the cryomodule to the first FFAG arc by passage through four independent spreader-chicane splitters, S1-4, and from the second arc back into the cryomodule via similar "combiners", T1-4.

Operating Cβ as an pre-injector – with no deceleration – is simpler. It becomes a Recirculating Linac Accelerator, providing continuous electron acceleration up to a maximum energy of 311 MeV, since a fifth pass through the cryomodule can be extracted to the accumulator. Time of flight adjustments are not necessary. FFAG optics using permanent magnets simplify the operation even further, and lower power consumption operating costs.

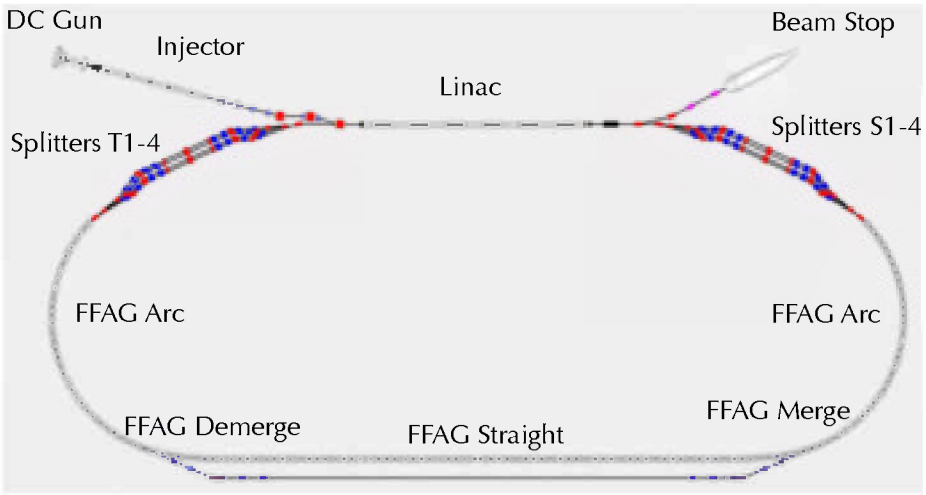

Figure 2.4: Layout of the Cornell-BNL FFAG Electron Test Accelerator, Cβ, in the energy recovery configuration envisaged for linac-ring FFAG prototyping [7]. Energy recovery is not necessary in prototyping a Cβ-style FFAG ring-ring pre-injector, with a maximum energy of about 311 MeV.

2.3.2 Section of the SLAC linac

It might be possible to recycle part of the SLAC warm linac, with the advent of a superconducting linac for LCLS-I and LCLS-II. This possibility was proposed by Zhang [3].

The SLAC linac operated at up to 30 Hz as a multi-turn injector for PEP-II [8]. Each pulse contained a single bunch of up to 9×10^{10} or 1.4 nC of electrons. Under nominal conditions the quantum efficiency had a 4 day lifetime. In the baseline scenario the eRHIC electron storage ring needs 330 bunches of 3×10^{11}

electrons, or 16 μC. It would take about 37 seconds to fill the electron storage ring from empty, assuming the maximum injection current could be used. Injection in PEP-II generally took a couple of minutes, for a comparable amount of total stored charge.

Full intensity bunches could be prepared by accelerating individual bunches up to an intermediate energy midway between spin resonances, for accumulation. The transverse radiation damping time is under 5 ms for a ring of 15 m radius and $\rho = 10$ m at 200 MeV. It takes about a second to accumulate a 50 nC bunch if the linac runs at 60 Hz. This full intensity bunch would be injected into the linac and accelerated to top energy. The stored energy requirements in the SLAC cavities and other beam loading related issues would need careful consideration before proceeding with this option. While the linac may be available for "free", this option would need about 1 km of tunnel to be constructed, including space for the klystron gallery and all ancillary equipment.

2.3.3 Figure-of-8 synchrotron

A figure-of-8 rapid cycling synchrotron with low beam current could be used to fill the storage ring in multi-turn mode.

Assuming that the bend angle in the arc of each lobe is 270°, and a tunnel radius of $r = 250$ m, the distance along the long axis of the figure-of-8 is approximately

$$w \;=\; 2(1+\sqrt{2})\,r \;=\; 1,207 \text{ [m]} \tag{2.1}$$

and the total circumference is approximately

$$C \;=\; (3\pi+4)\,r \;=\; 3,356 \text{ [m]} \tag{2.2}$$

This just fits inside the RHIC ring, with some space to spare.

Assuming a dipole bend radius of $\rho = 200$ m, the energy loss per turn is 106 MeV at 20 GeV. The required dipole fields and ramp rates compare favorably with those of the 60 Hz, 12 GeV Cornell synchrotron injector – robust rapid cycling magnets of this sort exist, and are inexpensive. The transverse radiation damping time at 2 GeV is about 5 ms and scales as γ^{-3}.

An installed RF voltage of 120 MV gives a synchronous phase of $\phi_s = 62°$ at 20 GeV. The currently unused warm LEP accelerating modules generate 25 MV over 20.4 m, powered by a 1.0 MW klystron. Five such modules could be used for the figure-of-8 RF system, filling 102 m of the total straight section length of 1000 m.

Bunch-to-bucket injection into adjacent RF buckets in the synchrotron could be used to prepare several bunches for simultaneous acceleration. Partial intensity bunches could be injected into the stable spin direction on different turns, and then accelerated to an intermediate energy where the radiation damping time is fairly short, but where the synchronous voltage in manageable. Higher intensity bunches can then be coalesced by performing a bunch merge and waiting for a few radiation damping times. The highest intensity bunches might need a few such coalescing steps, before being recaptured on a high power RF system for acceleration to top energy. Alternately, a small damper ring at 200 MeV could be used, as discussed above.

Even with a bunch charge of 50 nC the X-ray power is 0.47 MW at 20 GeV. This relatively low power, combined with the high voltage, suggests that superconducting RF might be worthwhile. Superconducting cavities would draw far less power, reducing perturbations to the electrical grid.

Polarization preservation

The primary unknown with the figure-of-8 injector option is the level of polarization preservation during acceleration. This needs more study, but some preliminary comments are possible.

With $f_{RF} = 450$ MHz, $\tan\phi_s = 2$, and momentum compaction $\alpha_p = 1/30^2$, the synchrotron tune is $Q_s = 0.0015$ at 2 GeV, and $Q_s = 0.048$ at 20 GeV. For a flat figure-of-8 the spin tune is exactly zero, making it prone to instabilities. A solenoid magnet can be used to create a non-zero spin tune albeit with

a non-vertical stable spin direction. Another potential way to preserve polarization comes from noting that the spin tune changes by 1 for each 440 MeV of energy gain for a circular ring. If all the accelerating cavities are limited to one straight, and some additional RF voltage is installed to counteracted some of that voltage in the other straight, a fixed energy difference can be maintained in the two lobes of the figure-of-8.

In either case significant studies remain to be performed.

2.3.4 Recirculating linac – warm or cold

The optimization of a recirculating linear accelerator (RLA) injector has been carried out as part of the linac-ring eRHIC design. The spin behavior is well understood and favorable. For the ring-ring design deceleration is unnecessary, simplifying the design. An average current of 50 μA and a repetition rate of 78 kHz with a charge of 0.64 nC per linac bunch leads to the need for 78 injection cycles to accumulate a 50 nC bunch. This implies that it takes about 0.8 seconds to replace a bunch, assuming a radiation damping time of about 10 ms. A residence time of 2.4 minutes if 180 bunches are unfavorably polarized – quite short compared to the half hour depolarization time. An accumulator would be used to prepare high intensity bunches, as with the "SLAC linac" option.

2.3.5 Injector risks

Of these three alternative injector scenarios, only one poses a significant risk – the figure-of-8.

Two scenarios – the "SLAC linac" and the CEBAF-style "recirculating linac" – use existing technology. The SLAC linac even uses existing hardware to accelerate transversely polarized electrons to 20 GeV. Polarization preservation in a recirculating linac with a small number of recirculations has been demonstrated at CEBAF. The SLAC linac can be considered to be an extreme case of a recirculating linac with only one recirculation, assuming that it is broken up into six separate sections that are installed in the six straight sections of the RHIC tunnel. Polarization is obviously preserved, as well, if the SLAC linac is installed in a separate, straight tunnel.

On the other hand, polarization preservation has not yet been experimentally demonstrated in a rapid cycling synchrotron, neither with a conventional layout nor in a figure-of-8 configuration. Success is expected to be more likely with a figure-of-8 layout. Nonetheless, preliminary simulations indicate that polarization is preserved up the acceleration ramp even in a conventionally shaped rapid cycling synchrotron.

More detailed simulation studies are required. Ideally, beam experiments could be carried out at the Cornell rapid cycling synchrotron.

Chapter 3

Lattices and optics

3.1 Interaction region requirements for Physics

Several Physics requirements need to be integrated into the interaction region design, in order to perform the physics program as described in the EIC White Paper [9] and in the RHIC Design Study [10]. These requirements are also described in detail on a dedicated page of the eRHIC-wiki [4]. The main requirements are described here.

Requirements in the outgoing hadron beam direction

To veto the breakup of nuclei in the reaction $e + A \longrightarrow e' + A' + VM$ it is critical to have a large acceptance for breakup neutrons at zero degrees. Simulations show that a ± 4 mrad cone needs to be passed undisturbed to the Zero Degree Calorimeter (ZDC) in order to detect these breakup neutrons efficiently.

To ensure exclusivity in deeply virtual Compton scattering (DVCS) reactions $e + p \longrightarrow e' + p' + \gamma$ it is critical to detect the forward going scattered proton, and to measure its transverse momentum very accurately. Figure 3.1 shows the scattered proton momentum versus its scattering angle in the laboratory frame. A common technique to detect these protons is to install Roman Pots symmetrically around the beam in the warm sections of the outgoing proton beam. A distance of 10 σ from the Roman Pot to the core of the beam is required for safety. The physics requirement is to detect protons with the smallest and largest possible scattering angles. This translates to a requirement on the 10 σ of proton beam divergence of less than 0.68 mrad at 250 GeV, and 1.7 mrad at 100 GeV. The maximum angle that needs to be transported through the system is 5 mrad at 250 GeV and 13 mrad at 100 GeV.

Note that the detector acceptance starts only at 20 mrad.

Requirements in the outgoing lepton beam direction

To match the high statistical precision that an EIC will achieve for basically all key measurements, it is extremely important to reduce systematic uncertainties. Most critical is the bunch-by-bunch measurement of luminosity using bremsstrahlung events $e + p/A \longrightarrow e' + p'/A' + \gamma$. The requirements are to know the absolute luminosity to better than 1% and to determine the relative luminosity to 10^{-5}. Simulations of this fully calculable process show that the natural angular distribution of the bremsstrahlung photons is contained in a cone of 0.05 mrad. The width of the bremsstrahlung photon cone that is to be transported through the interaction region at zero degrees is purely given by the electron beam divergence.

It is critical to detect the scattered lepton below a Q^2 of 0.1 GeV^2, the limit seen in the main detector. In order to do so it is necessary to install a special electromagnetic calorimeter to detect leptons scattered with very small scattering angles. This calorimeter needs to be installed after a bend of the lepton beam, so that the scattered leptons are separated from the main core of the outgoing electron beam. It is critical

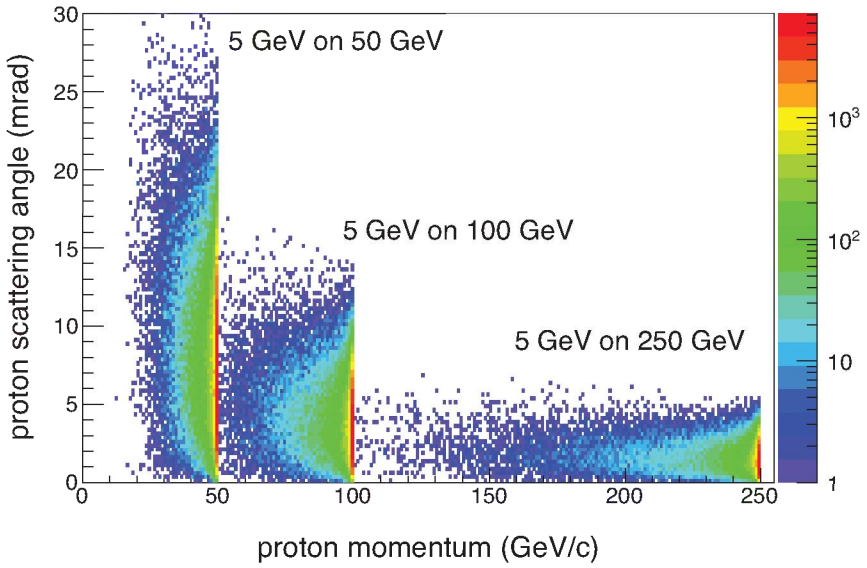

Figure 3.1: The scattered proton momentum versus scattering angle in the laboratory frames for deeply virtual Compton scattering (DVCS) events with different beam energy combinations. The following cuts have been applied: 1 GeV^2 < Q^2 < 100 GeV^2, $0.00001 < x < 0.7$ and $0 < t < 2$ GeV^2. The angle of the recoiling hadronic system is directly and inversely correlated with the proton energy. It thus decreases with increasing proton energy.

to suppress synchrotron radiation hitting the calorimeter as much as possible. Leptons with Q^2 values as small as 10^{-4} can be detected in the linac-ring design.

Requirements in the incoming lepton and hadron beam directions

A lepton beam polarimeter needs to be located before the experiment between the spin rotators, in order to verify that the polarization vector is fully rotated to the longitudinal. It might be also be beneficial to measure polarization right after the experiment, in order to diagnose the possibility that the polarization is compromised by other depolarization effects during the collision.

3.2 Interaction region design

The nominal interaction region layout shown in Figure 3.2 has ±4.5 m of free space around the interaction point available for a central detector, and 2 m of free space available for Roman Pots between the dipoles of the dogleg that bends the (blue) proton beam in the horizontal plane. In particular, Figure 3.2 illustrates four of the five angles that are vital in interaction region design, with their nominal (or typical) values:

1. The neutron cone angle $\theta_n = \pm 4.0$ mrad is shown in green. The region within an angle of $\pm\theta_n$ of the proton direction at the interaction point – the horizontal axis in the figure – is used for detector instrumentation, and must remain clear of accelerator equipment. It may be possible to reduce this angle to 3 mrad [4].

2. The horizontal crossing angle $\theta^* = 15$ mrad between the electron (red) and proton (blue) directions separates the beams into two optical channels, and suppresses long-range beam-beam interactions. The luminosity lost to the crossing angle is largely restored by crab cavities, not shown in Figure 3.2.

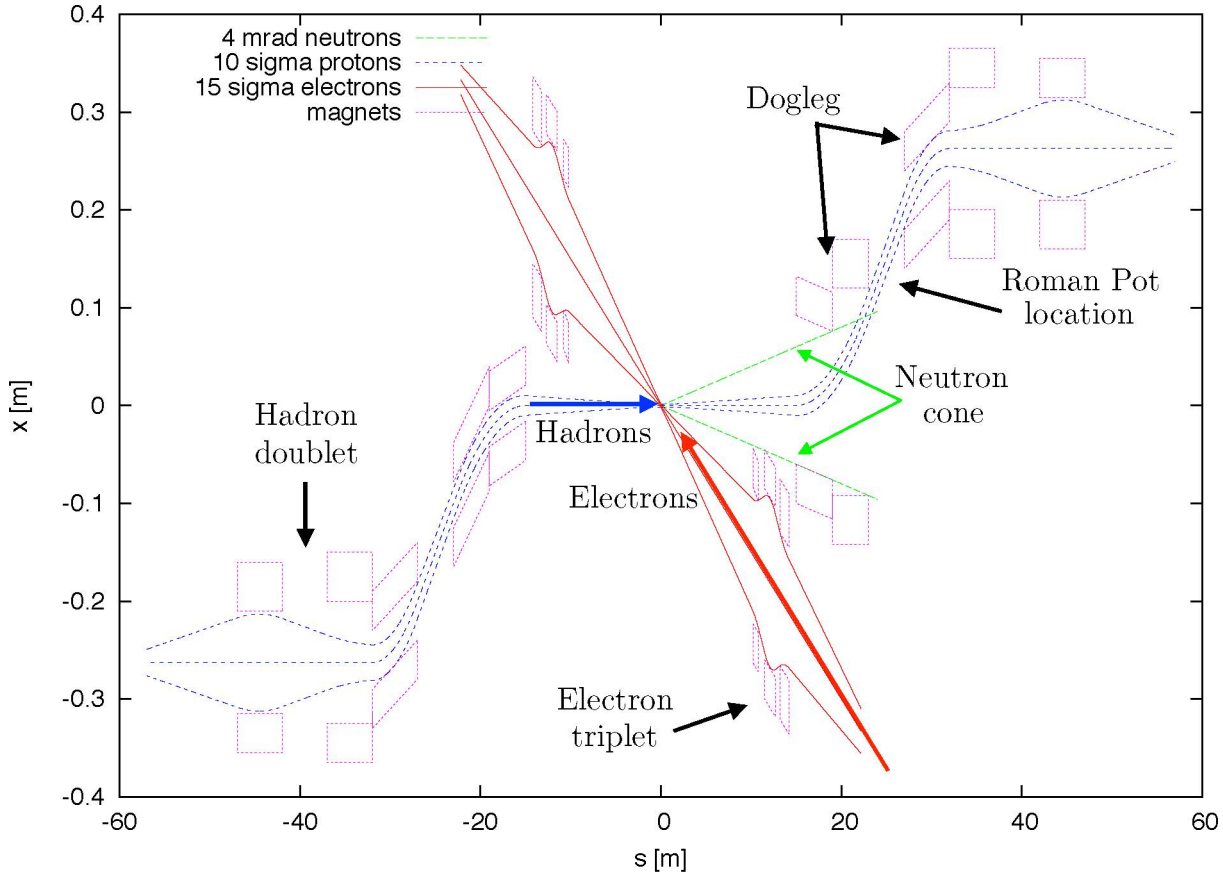

Figure 3.2: Interaction region layout (top view) with a full proton beam dogleg. Roman Pots are placed between the dipoles of the dogleg that bends the (blue) proton beam in the horizontal plane.

3. The rms electron divergence angle

$$\sigma_e'^* = \sqrt{\frac{\epsilon_e}{\beta_e^*}} \tag{3.1}$$

and the rms proton divergence angle

$$\sigma_p'^* = \sqrt{\frac{\epsilon_p}{\beta_p^* \gamma_p}} \tag{3.2}$$

may both be different in the two planes, depending on the horizontal and vertical values of the **unnormalized** emittance ϵ_e, the **normalized** emittance ϵ_p, and β^*, and the Twiss functions at the interaction point. Figure 3.2 shows the geometric layout based on minimum apertures of $\pm 15\,\sigma_e'^*$ (red) and $\pm 10\,\sigma_p'^*$ (blue) in their respective channels.

4. The proton transverse momentum acceptance angle

$$\theta_{p\perp} = \frac{200\ [\mathrm{MeV/c}]}{P_p} > \frac{200\ [\mathrm{MeV/c}]}{250\ [\mathrm{GeV/c}]} = 0.8\ [\mathrm{mrad}] \tag{3.3}$$

corresponds to the minimum deflection angle that should be detectable in the Roman Pots. Such a proton should be sufficiently far in the tails of the proton beam, a condition that is satisfied if

$$\theta_{p\perp} > 10\,\sigma_{pH}'^* \tag{3.4}$$

in both horizontal and vertical planes.

3.2.1 Interaction region optics and magnets

Focusing of both electron and hadron beams is provided by superconducting magnets. The low-β electron triplet is located 10.2 m from the interaction point. At this location there is sufficient separation for the magnet coils and steel to be placed between the 15 σ electron beam and the 4 mrad neutron cone, thus requiring only a relatively small magnet aperture. In addition, the 5.7 m long drift section from the triplet at 10.2 m to the central detector at 4.5 m provides a lever arm that permits the installation of synchrotron radiation masks at the entrance to the detector, to collimate the synchrotron radiation fan generated by the triplet quadrupoles. The remaining narrowed photon fan then passes safely through the central detector into the downstream electron beamline, where it grazes the inner wall of the vacuum pipe further downstream. Additional masks will be placed in this downstream beamline to minimize backscattering of these photons into the central detector. Table 3.1 lists the design parameters of the individual quadrupoles in the electron low-β triplet.

Quadrupole	**Length** [m]	**Strength** [m^{-2}]	**Aperture radius** [mm]	**Peak field** [T]
Electron triplet				
QE1	0.6	-0.43	70	2.1
QE2	1.2	0.43	87.5	2.5
QE3	1.0	-0.30	68	1.4
Proton doublet				
QP1	5.0	-0.022	62	1.14
QP2	5.0	0.026	52	1.13

Table 3.1: Design parameters of the interaction region low-β quadrupoles. The length of the drift spaces between the electron quadrupoles is 0.5 m, to allow tapering of the beampipes between the magnets according to their different diameters. Electron apertures and peak fields are based on a 20 GeV electron beam and a minimum aperture of 15 σ. Proton apertures and peak fields are based on a 250 GeV proton beam and a minimum aperture of 10 σ. The length of the drift space between the two proton quadrupoles is 5 m.

The proton low-β doublet is located 32 m from the interaction point. Crab cavities are installed on both ends of the horizontally focusing quadrupole QP2. To minimize the required crab cavity voltage, the horizontal β-function is maximized there. The magnet apertures are listed in Table 3.1, based on a 10 σ aperture for a 250 GeV proton beam. However, it is desirable to increase these apertures, to allow focusing of lower energy beams with their associated larger emittances, achieving the same β-functions at the collision point. Increasing the aperture by a factor two or even three is feasible and should be considered, thanks to the low gradient of those quadrupoles.

Separation of the proton beam from the neutron cone is provided by a set of dipoles forming a dog leg upstream of the low-β doublet. The innermost dipole consists of two individual magnets of 4 m length each, the first one of which is tilted in the horizontal plane to maximize the distance between the coils and the electron beam. The electron beam passes just outside the cold mass of this dipole; the magnetic field in this region is reduced to a few Gauss by means of additional coils. The 4 m long drift space between the two bends of the dogleg allows installation of Roman Pots for the detection of protons with a transverse momentum as low as 200 MeV.

3.2.2 Crab cavities or a dipole field in the detector?

The two colliding beams have to be separated from each other close to the detector to avoid parasitic beam-beam collisions, and to guide them into their respective focusing channels. Since the electron low-β quadrupoles generate synchrotron radiation due to their focusing fields, high energy photons must pass through the central detector. A masking scheme is required to collimate this photon fan to a manageable size before it enters the detector beampipe.

The entire 15 σ electron beam has to be completely separated from the proton beam and from the 4 mrad neutron cone at the entrance to the central detector, 4.5 m from the interaction point, where the synchrotron radiation masks are installed. The required separation of 67.5 mm can be accomplished by using either a crossing angle, or a dipole field over the length of the central detector.

Crab cavities are required to restore the luminosity loss when a crossing angle is used. A crab cavity voltage of $V_{crab} = 7.4$ MV is needed at a frequency of $f_{crab} = 168$ MHz when the total horizontal crossing angle is 15 mrad, in optics with $\beta_x^* = 2.18$ m at the interaction point and $\beta_{x,crab} = 2400$ m at the crab cavities. This restores 75% of the head-on luminosity for proton bunches with an rms length of $\sigma_s = 20$ cm.

Alternatively, separation can be achieved by a dipole field in the central detector. To achieve the same separation at the entrance to the central detector a net bending angle of 30 mrad must be generated over the 4.5 m length, requiring a bending radius of 150 m. This generates 255 kW of synchrotron radiation with a critical photon energy of 120 keV when the electron beam energy is 20 GeV. The large horizontal width of this photon fan prevents detector elements being placed close to the beam.

The main concern is that the fan will be very wide, though reasonably flat, with a horizontal opening angle of 30 mrad, starting 10 m from the interaction point. At the entrance of the detector it will therefore be 300 mm wide, and at the exit will grow to 570 mm. The height of this fan is essentially the same as the electron beam height, since that is the closest that collimators can be placed. A wide fan will inevitably hit "something" on the downstream side of the detector, like the crotch that separates the electron and proton beams. Photons will backscatter from there. The fan will also hit and potentially quench the superconducting electron quads on the downstream side, because collimation is inefficient with large critical energies of about 120 keV.

It is conceivable that an interaction region can be designed with a dipole field in the detector instead of crab cavities, but the design would be challenging. For this reason the rest of this report focuses solely on an interaction region layout with a crossing angle and crab cavities.

3.2.3 Backgrounds and the influence of high bunch frequencies

It is extremely important to minimize experimental backgrounds during high precision measurements. Synchrotron radiation from the electron beam is the dominant source of background in an electron-ion collider, although there are other important mechanisms. Reliable calculations of the synchrotron radiation load in the interaction region are necessary, in order to evaluate how well the different detector technologies will be able to tolerate the synchrotron radiation background.

Insofar as a ring-ring design needs more integrated current to reach the same luminosity as a linac-ring design, the integrated synchrotron radiation rate will also be higher.

For a high frequency bunch crossing rate it is important that the crossing angle is large enough to separate the beams so that there is no chance for more than one bunch interaction in the interaction region.

The second most important source of background is beam-gas events, in which protons or ions interact with the gas remaining in the beampipe. Table 3.2 shows the results of a calculation of beam-gas event rates, compared to the rate of true e+p or e+A events, for both ring-ring and linac-ring designs. An accurate estimation of beam-gas event rates depends on the detailed pressure distribution in, and close to, the interaction region. There tends to be a high acceptance from events at a significant distance upstream of the detector, because the kinematics are essentially those of a fixed target experiment.

The following assumptions have been made:

- The vacuum pressure is 10^{-9} mbar, similar to pressures achieved at HERA [11].

Event type	Linac-ring	Ring-ring
Deep inelastic scattering	40.6	2815
Bremsstrahlung	1	3.6
Beam gas (proton beam)	177	2657

Table 3.2: The average number of bunch crossings in the interval between events of different types. Deep inelastic scattering (good) events occur at approximately the same interval as beam-gas (bad) events. The beam gas events are given for a beampipe at room temperature and only for the part of the beampipe sitting in the detector

- The beampipe is at room temperature. This is inaccurate at least in the vicinity of the cold superconducting interaction region magnets
- The average atomic weight for the beam gas is $\langle A \rangle = 40$, equivalent to Argon.
- The beampipe is 10 m long, for a density of 2.65×10^{10} molecules/cm^2.
- The luminosity in the ring-linac design is 4.1×10^{33} cm^{-2} s^{-1}, with a proton bunch population of 3×10^{11} and a bunch spacing of 100 ns.
- The luminosity in the ring-ring design is 3.0×10^{33} cm^{-2} s^{-1} for 5591 bunches, with a bunch spacing of $\sim$2 ns, and a proton bunch population of 2×10^{10}.
- 20 GeV electrons are in collision with 250 GeV protons.

If the beampipe temperature is colder than room temperature, the beam-gas event rate increases by a factor of $T_{room}/T_{Beampipe}$. At room temperature there is one beam-gas event per deep inelastic scattering event in the ring-ring case, a rate that is tolerable. However, any increase will make separating real events from background events more difficult, especially for the high bunch frequency case.

3.3 Electron ring arcs

Two options for the arc cells – FODO and the Triplet Achromat Lattice (TAL) – are presented and compared in some detail in Appendix B [12, 13]. Summary results for unnormalized emittance and amplitude dependent detuning are presented here, as a function of the horizontal phase advance per cell in each case.

In both FODO and TAL cases the dipole radius of curvature is about 300 m. There are 11 FODO cells in each of the 6 arcs, or 12 TAL cells, leading to cell lengths of 29.62 m or 27.15 m, respectively. Shorter arc cell lengths are possible, needing more cells per arc. This would reduce the packing factor, and would require a smaller dipole bending radius to fit in the existing tunnel. Thus, the selection of the number of cells per arc is a compromise between increasing the linear power density of the synchrotron radiation, and reducing the unnormalized emittance.

Dependence on the phase advance per cell

Figure 3.3 shows the variation of the horizontal unnormalized emittance with the horizontal phase advance per cell at three electron energies – 5 GeV, 10 GeV, and 20 GeV – in a lattice dominated by arc cells.

Similarly, Figure 3.4 shows the variation of the detuning coefficients $\alpha_{x,x}$, $\alpha_{x,y}$, $\alpha_{y,x}$, and $\alpha_{y,y}$ with the phase advance per cell, where

$$\alpha_{i,j} = \frac{dQ_i}{dJ_j} \tag{3.5}$$

J_x and J_y are the horizontal and vertical actions, and i and j are either x or y. In both Figures 3.3 and 3.4 the behavior with FODO cells is shown at the top, and with TAL cells at the bottom.

Unnormalized emittances

Achieving the required unnormalized emittance becomes relatively more difficult at the lower operating energies, requiring a lower horizontal phase advance per cell. Due to the large variation of the dispersion at these different energies, matching the arc optics into the interaction regions requires significant operational flexibility.

Figure 3.3 shows that FODO cells achieve a 53 nm unnormalized emittance at 20 GeV with a horizontal phase advance of 123.6° per cell (and 90° vertical phase advance per cell) when the FODO cell has a bending magnet radius of 300.6 m. TAL cells with a bending magnet radius of 293.1 m achieve a 53 nm unnormalized emittance at 20 GeV when the horizontal phase advance per cell is 98.3°.

Amplitude detuning

Figure 3.4 shows the amplitude detuning coefficients $\alpha_{i,j}$ due to the sextupoles that are necessary for chromaticity correction. The coefficient $\alpha_{x,x}$ becomes singular when the horizontal phase advance per cell $\Delta\phi_x$ approaches 120°, because perturbation theory predicts that

$$\alpha_{x,x} \sim \frac{1}{\sin(3\Delta\phi_x)} \tag{3.6}$$

Superficially, this singularity is a problem at 20 GeV for the FODO cell option, because the nominal horizontal phase advance per cell is 123.6°. This probably also reduces the dynamic aperture significantly.

The detuning coefficients for the TAL cells are in general larger than those for the FODO cells, although they are smaller with the horizontal phase advance per cell of 98.3° that is nominally required for 20 GeV operation.

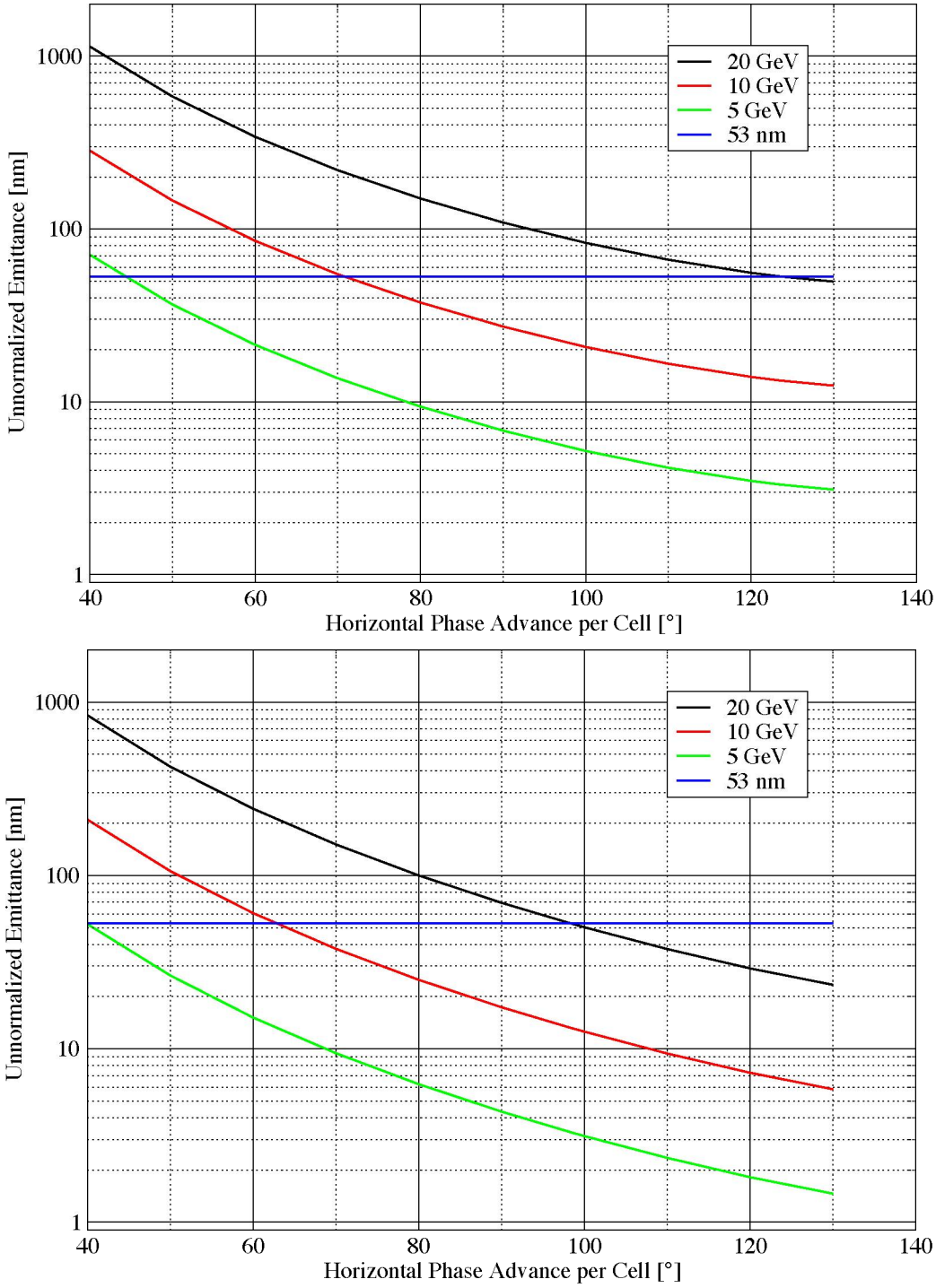

Figure 3.3: Unnormalized electron emittance versus phase advance per cell at three energies. TOP: FODO cells. BOTTOM: TAL cells. The blue lines show a reference 53 nm emittance.

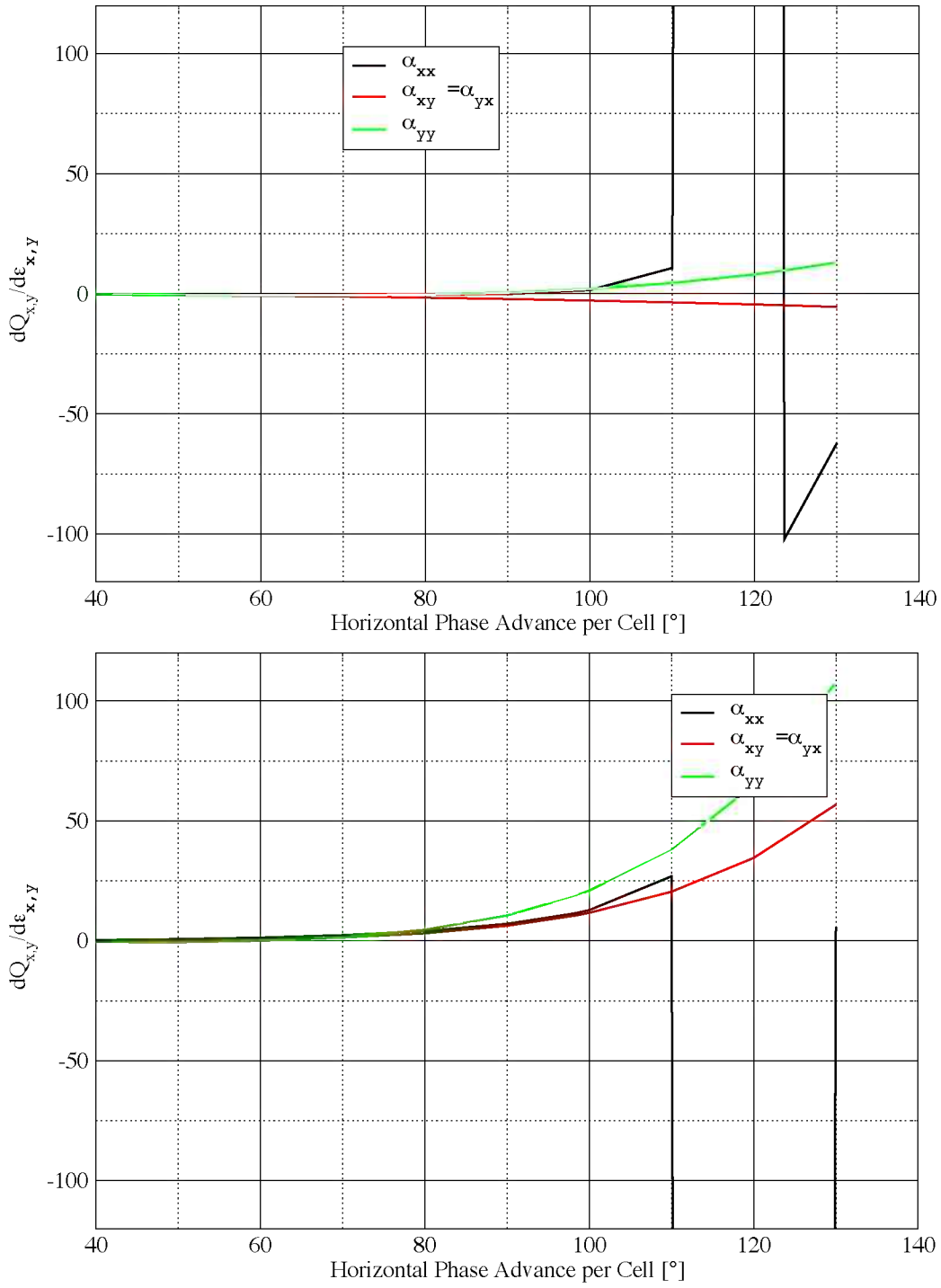

Figure 3.4: Amplitude detuning coefficients versus phase advance per cell at three energies. TOP: FODO cells. BOTTOM: TAL cells. The singularity at $\Delta\phi_x = 120^\circ$ is due to a $\sin(3\Delta\phi_x)$ resonance denominator.

Chapter 4

Beam physics

4.1 Path length and damping decrement control

The protons or ions in eRHIC will have energies ranging from 50 GeV/u through 250 GeV/u. For the eRHIC circumference, the difference in orbital period per turn over that energy range is about 2.16 ns. The variation in the electron velocity is negligible, so to keep bunch collisions synchronized, the path length of one or both beams must be changed.

This process is complicated by the desire to increase the damping decrement by increasing the synchrotron radiation – up to a maximum average of 10 kW/m in the arcs – over the entire range of electron energies, so as to maximize the beam-beam tune shift allowed for the electron beam. For 20 GeV electrons, this is accomplished by having dipoles with fields of 0.22 T (300 m bending radius for 20 GeV electrons). To produce sufficient radiation for lower energy electrons, the dipoles will be split into parts, with different parts having different fields (when electron energies are below 20 GeV). To achieve a desired bend angle, the desired amount of radiation, and maintain symmetry, each dipole will be split into a minimum of three parts. It may be desirable to split the dipole into more parts as discussed below. The beam will always be steered through the centers of the quadrupoles. The beam will, however, be offset in the dipoles. Thus the dipoles are expected to have a relatively wide aperture (but still a modest vertical aperture). We will keep the dipoles fields at 1.2 T or less to avoid saturation effects, though this will require some dipole fields to be negative at the lowest electron energies.

When the different parts of the dipoles have different fields, the orbit length will be longer than the case where all parts have the same field. This is generally desirable, since at lower proton energies, the length of the electron orbit must be increased. However, this path length must be precisely chosen based on the proton energy, while the dipole field pattern is at least partially determined by the electron beam energy. Splitting the dipoles into at least 5 parts will give the required free parameters to independently control the total bend angle, the amount of radiation generated, and the path length increase. However, the path length increase will likely far exceed the desired values, at least with only 5 parts in each dipole and with lattices similar to those described in Section 3.3 and Appendix B. We will probably not be able to bring the path length to the desired values while keeping the dipole fields to reasonable values. We expect that this could be remedied with an increased number of parts in each dipole.

The total path length difference between 50 GeV protons and 250 GeV protons is 65 cm. However, one case we will need to deal with is 100 GeV/u ions colliding with 20 GeV electrons. Since 20 GeV electrons must also collide with 250 GeV protons, and since the radiation limitation means that we cannot increase the path length of the 20 GeV electrons using segmented dipoles, we must find another mechanism for correcting the 14 cm path length difference between 250 GeV protons and 100 GeV/u ions.

This additional path length difference will be created using the hadron ring. The RHIC arcs contain two rings, an inner and an outer ring. There is a substantial path length difference between these two rings. We will operate the hadron ring by having the beam pass through three inner and three outer rings. However, we will be able to select any combination of three inner rings and three outer rings. If the path

length in all the outer rings is the same, but the path lengths in the inner rings are L, L, $L+\Delta$, $L+2\Delta$, $L+4\Delta$, and $L+8\Delta$, then by selecting various combinations of 3 inner and 3 outer rings, one can have a path length anywhere from $6L+\Delta$ to $6L+14\Delta$, in steps of Δ, from the inner rings. If we can steer the beam in the RHIC arcs to vary the path length over a range of Δ, then any path length over a range of 14Δ can be achieved in the hadron ring.

At a minimum, the hadron ring can easily create a 14 cm path length difference with a Δ of only 1 cm. It can be used to create additional path length difference should it be difficult or expensive to completely control the path length using the dipoles in the electron arc. We expect from initial experiments that beam steering should be able to accomplish a path length difference of at least 5 cm, which by itself would allow a continuous path length correction of 70 cm; a larger range could be accomplished if one does not insist on being able to choose any particular path length in the hadron ring.

4.2 Electron polarization

The achievable beam polarization level in electron circular accelerators is defined mostly by two processes related with synchrotron radiation: Sokolov-Ternov self-polarization and depolarization caused by synchrotron radiation quantum emission. The self-polarization process leads to a slow build-up of electron polarization in the direction opposite to the vertical guiding field, up to a maximum level of 92.4% in an accelerator without spin rotators and with sufficiently weak spin resonances.

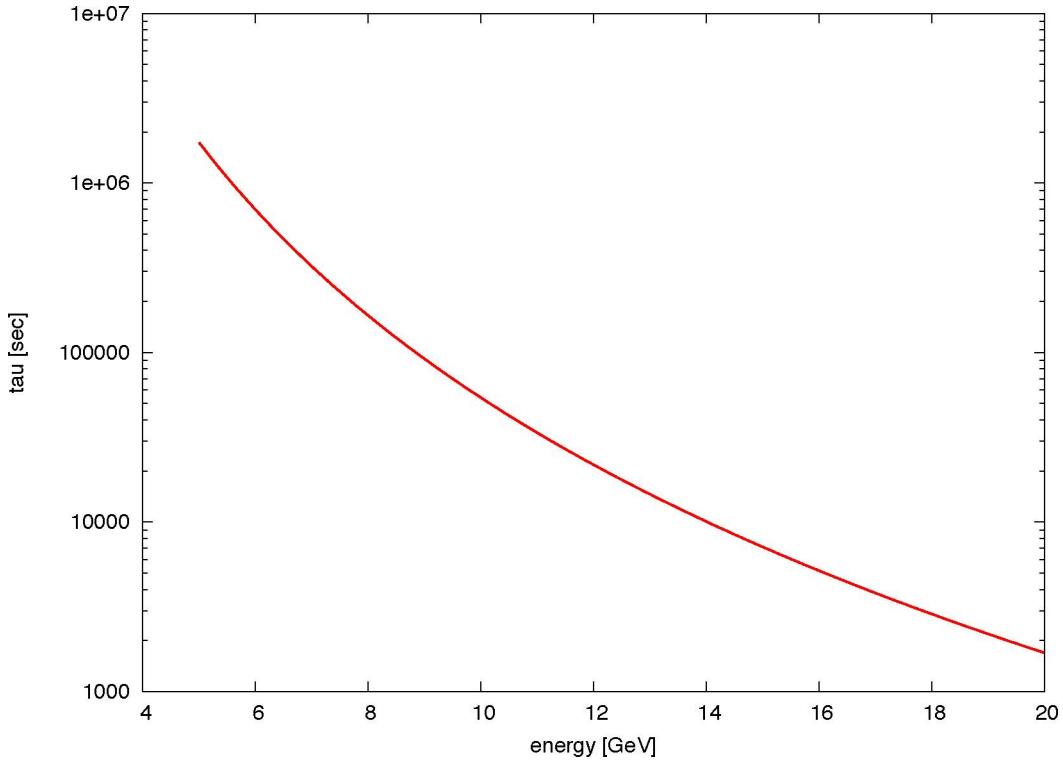

Figure 4.1: Sokolov-Ternov polarization time in the eRHIC electron storage ring as a function of energy.

However, the presence of spin rotators, wigglers, as well as strong spin resonances reduces the achievable polarization level. An important quantity is also the self-polarization time, which has a strong dependence on the beam energy, scaling like E^{-5}. The self-polarization time for an eRHIC storage ring in the energy range of interest is shown in Figure 4.1. The self-polarization time is long over practically all of energy

range, except approaching 20 GeV where it drops to about 30 minutes. This demands a full energy polarized electron injector, so that the electron beam is injected into the storage ring with high polarization - 70% to 80%. One benefit of the long self-polarization time is that spin patterns containing bunches of opposite polarization orientation can be used - see Section 4.2.2.

The main challenge of spin dynamics in the storage ring is to preserve the high polarization level of the injected beam, at least at energies that are far from spin resonance conditions. The required timescale of polarization preservation is defined by the time interval between electron beam re-injections. Depolarizing effects are dominated by spin diffusion caused by the quantum nature of synchrotron radiation emission. In the presence of synchrotron radiation related spin diffusion the equilibrium polarization is described by the Derbenev-Kondratenko formula [14]. The depolarizing time τ_{depol} is defined by the diffusion rate of beam energy spread and the sensitivity of the stable spin solution n to the particle energy.

$$\frac{1}{\tau_{depol}} = C \left\langle \left| \gamma \frac{\partial \mathbf{n}}{\partial \gamma} \right|^2 \frac{d(\delta\gamma/\gamma)^2}{dt} \right\rangle_\theta \tag{4.1}$$

where C is a constant defined by other fundamental constants and γ is the relativistic factor. The averaging inside angle brackets $\langle\rangle$ is done over accelerator azimuth θ and, in general, over the beam phase space.

The strength of depolarising effects increases in general as E^7, thus making it a bigger challenge for higher energy circular accelerators to maintain high polarization. Nonetheless, Figure 4.2 shows that several accelerators operating above 10 GeV have achieved high electron polarization levels, exceeding 60% [15]. The accelerator techniques used to achieve high polarization at high energies included highly-efficient orbit correction, beam-based alignment of Beam Position Monitors relative to quadrupole field centers, and harmonic spin matching [16]. These tools are related to mitigating the effects of imperfection spin resonances, and their synchrotron sidebands.

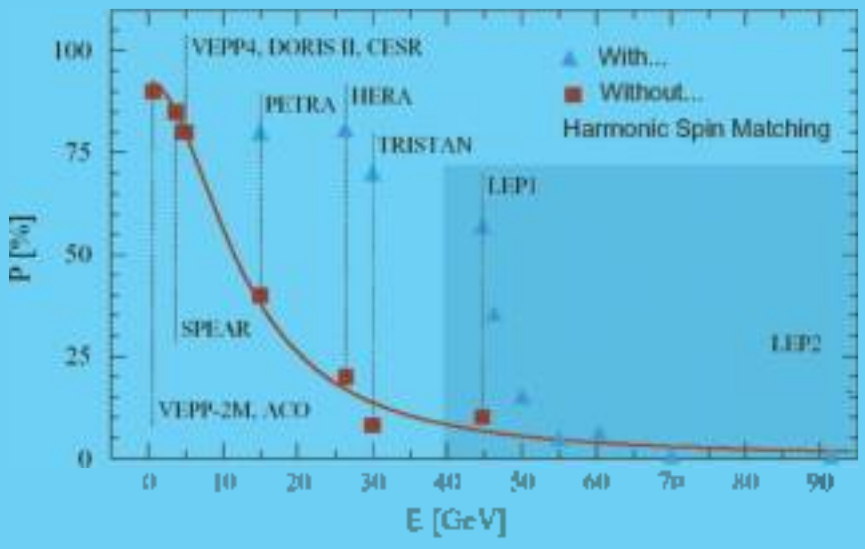

Figure 4.2: Electron polarization levels achieved in various circular circular electron storage rings [15].

In addition, intrinsic resonances must be narrow enough to preserve high polarization, at least at energies far enough away from spin resonance conditions. Betatron coupling and unmatched spin rotator insertions can considerably widen the spin resonances, decreasing the achievable polarization. Thorough spin simulation studies have yet to be performed, to determine the tolerances on the orbit and on betatron coupling control, and the required efficiency of spin matching and correction techniques.

The storage ring uses damping wigglers to increase the damping decrement at lower energies, and to adjust the electron path length. Wiggler-enhanced synchrotron radiation increases the spin diffusion

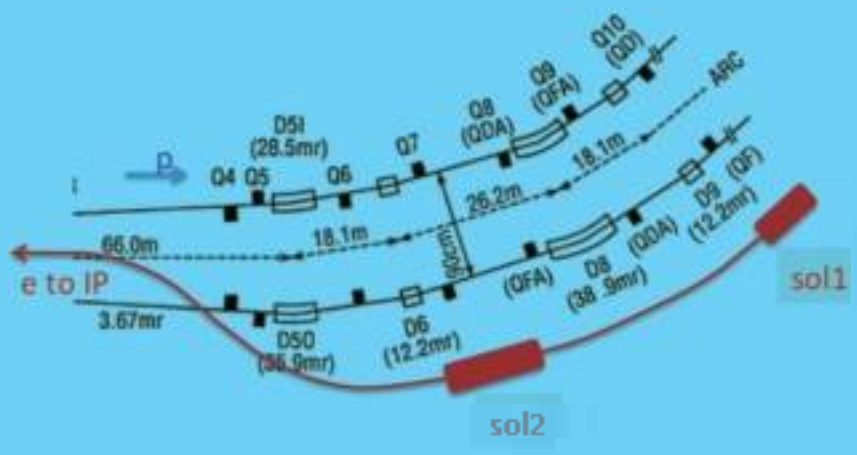

Figure 4.1 Layout of the electron spin rotators

rate. Thus, careful attention must be paid to the possibility of enhanced depolarization at beam crossings. Similarly, the effect of beam-beam interactions on polarization needs attention, since large electron beam time spreads would effectively widen the intrinsic resonances.

4.2.1 Spin rotators

Spin rotators are needed to convert the vertical polarization of the electron beam in the arcs to a longitudinal polarization at the experimental detector. The state of the art electron spin rotator that was used in the electron proton collider HERA (820 GeV) [Bernardini 67] was a superb example of interleaved vertical and horizontal dipole magnets to transform the vertical spin of 27.5 GeV electrons to the required orientation in the horizontal plane. The vertical orbit excursions inside the spin rotator were quite large – about 20 cm. This requiring some of the rotator magnets to be shifted vertically from the plane of the HERA electron ring.

Parameter		sol1		sol2	
Energy range	GeV	3	10	10	20
Field integral range	T m	26	53	52	105
Length (at 7 T)	m	7.6		13.0	
Orbit angle from the IP	mrad	92		46	
Location in the RHIC tunnel		D9	D10	D6	Q8

Table 4.1 Spin rotator parameters

The eRHIC spin rotators must operate over a large energy range, from 5 GeV to 20 GeV. Since the orbit excursions in the dipole magnets scale inversely with the beam energy, a HERA type rotator leads to large vertical excursions of 5 GeV electrons. Further, the synchrotron radiation power (per meter) produced by 20 GeV eRHIC electrons is considerably larger than the 27 GeV electrons in HERA, due to the much larger electron current. Reducing the linear power load requires further increasing the rotator length and, correspondingly, the vertical orbit excursion. Therefore, the only practical solution is a spin rotator based on strong solenoid magnets. Solenoidal Siberian Snakes have been used at electron accelerators operating

in the 0.5 GeV to 1 GeV range [18]. The integrated longitudinal field necessary to rotate the electron spin by 90 degrees, from the vertical to the horizontal, is

$$BL\,[\mathrm{Tm}] = 5.240\,E\,[\mathrm{GeV}] \tag{4.2}$$

A solenoid-based scheme for eRHIC using two rotators is shown in Figure 4.3. The first rotator (sol1) is used for operations in the 5 GeV to 10 GeV energy range. A second rotator (sol2) is also excited in the 10 GeV to 20 GeV energy range. The total spin rotation produced at any energy is 90 degrees. Each spin rotator contains two solenoids, and at least 5 skew quadrupoles to compensate for the betatron coupling and the vertical dispersion. Table 4.1 lists the main parameters of the rotators. The maximum field integrals of 53 Tm and 105 Tm can be realized by using superconducting magnets with fields in the 7 T to 10 T range. High temperature superconducting technology might be used to produce even higher fields.

Perfect longitudinal polarization at the interaction point is only achieved at 7.5 GeV and 15 GeV, in the suggested scheme. Figure 4.4 shows the slight deviations of the polarization orientation that occur at other energies, with a worst case longitudinal spin projection reduction of 13%.

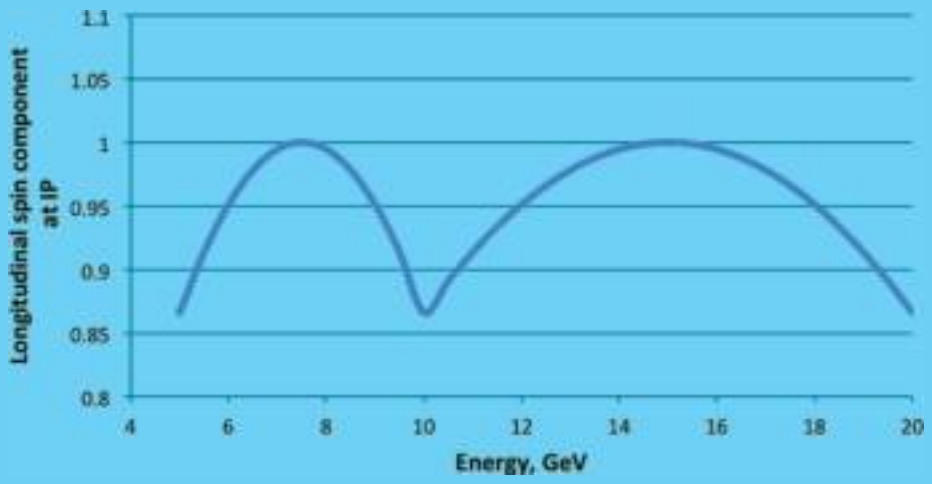

Figure 4.4: Deviation of the polarization orientation as a function of energy.

Spin matching conditions on the beam optics have to be established and satisfied in order to minimize the depolarization effects caused by synchrotron radiation induced diffusion. The future evaluation of depolarizing effects and spin matching must include the effect of the detector solenoid, with an integrated strength in the 4 Tm to 5 Tm range. In general, spin matching conditions with solenoid spin rotators will be energy dependent. The machine optics must satisfy them at all electron energies in the range from 5 GeV to 20 GeV.

4.2.2 Spin flipping

To realize arbitrary spin patterns in the electron beam, electron bunches with spins up and down need to be injected into the eRHIC electron storage ring. In bunches with spin "down" single electrons will flip their spin to the "up" direction, with the Sokolov-Ternov time constant shown in Figure 4.1. This will effectively depolarize those bunches. Entire bunches (or bunch trains) need to be replaced on a regular basis. This suggests that electron injection will look exactly the same as proton injection – on-orbit and on-energy. In this scenario there should not be any significantly enhanced background in the detectors due to electron injection.

With the shortest Sokolov-Ternov polarization time of about 1600 seconds at an energy of 20 GeV, continuously replacing single bunches at 1 Hz would take 6 minutes for a 360-bunch fill. In reality it is sufficient to only replace those bunches with spin "down", which would only take 3 minutes. This

is sufficiently short compared to the Sokolov-Ternov polarization time, so that depolarization of those bunches is small even at 20 GeV.

Electron bunch intensity accumulation is necessary in the injector system if full-intensity bunches are to be injected into the storage ring, since the required intensity is about a factor of five larger than the intensity of the linac-ring Gatling gun design. This accumulation could be performed either in a rapid cycling synchrotron, or in a separate accumulator/damping ring, if a linac injector scheme is chosen. Such a dedicated accumulator/damping ring might be installed in the existing AGS tunnel.

4.3 Magnetized electron cooling

The electron cooling technique uses a co-propagating electron beam in a localized portion of a circular ion accelerator to obtain high-intensity ion beams with low momentum spread. Its underlying physical mechanism is the dynamical friction experienced by individual ions moving in the co-propagating electron distribution.

Existing electron cooling systems are based on an electron beam generated with an electrostatic DC electron gun, immersed in a longitudinal magnetic field. For cooling of 50 GeV to 250 GeV protons one needs 27 MeV to 136 MeV electrons, respectively. This makes electrostatic acceleration unviable. RF acceleration of a bunched electron beam results in an electron transverse momentum spread that is significantly larger than in existing electrostatic coolers. However, for cooling purposes, the large transverse temperature of electrons can be controlled with a strong magnetic field in a solenoid in the cooling section.

The presence of a strong longitudinal magnetic field changes the collision kinetics significantly. In the limit of a very strong magnetic field, the transverse degree of freedom does not take part in the energy exchange, because collisions are adiabatically slow relative to the Larmor oscillations. As a result, the efficiency of electron cooling is determined mainly by the longitudinal velocity spread of the electrons. Such "magnetized cooling" is extremely useful in obtaining high-brightness hadron beams at low energies.

Electron cooling times scale as A/Z^2, where A and Z are the ion atomic and charge numbers. This shows that proton cooling is less effective than heavy ion cooling. Electron cooling times grow rapidly with beam energy, making direct cooling of high energy protons ineffective, and suggesting a two-stage cooling for high-energy protons in which pre-cooling is first performed at a low energy.

Cooling becomes more rapid at low proton energies in the range 25 GeV to 50 GeV, and can be used to control or pre-cool transverse and longitudinal beam emittances to the required values. For example, cooling times of the order of 30 minutes should be possible at a proton energy of 50 GeV, with a magnetized cooler employing electron bunches with charges of about 10 nC, in a cooling section 40 m long that contains 2 T to 3 T solenoids. Such strong magnetic fields control the transverse temperature of the electrons, so the transverse emittance of the electron bunches can be relatively large.

If proton cooling is required at 250 GeV in an upgrade scenario, the proton emittance should first be pre-cooled at low energy. This is because electron cooling time scales like the cube of the rms velocity spread of the ions, making "hot ion" cooling too slow at high energies.

4.4 RF gymnastics

With voltages of order 100 MV and x-ray power of order 25 MW the energetics of the RF system need careful scrutiny. Figure 4.5 illustrates the situation. We assume assume time dependence $\exp(j\omega t)$ and work with amplitudes. The net current and voltage across the cavity obey

$$(I_F - I_R - I_B)Z_C = V \tag{4.3}$$

where we note that the image current of the beam, which is the negative of the beam current, is responsible for driving the cavity. The voltage across the cavity is equal to the voltage on the transmission line driving the cavity, evaluated after the transformer

$$(I_F + I_R)Z_0 = V \tag{4.4}$$

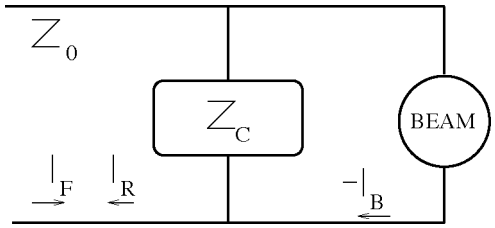

Figure 4.5: Circuit diagram for RF energetics.

Eliminating I_R yields

$$2I_F - I_B = V\left(\frac{1}{Z_C} + \frac{1}{Z_0}\right) \tag{4.5}$$

We have

$$\frac{1}{Z_C} = \frac{1}{R} + j\frac{Q}{R}\left(\frac{\omega}{\omega_r} - \frac{\omega_r}{\omega}\right) \tag{4.6}$$

where we have introduced the shunt impedance R, quality factor Q and (angular) resonant frequency ω_r.

We choose the cavity resonant frequency to cancel the reactive part of the beam current in eq (4.5). We take the convention that the synchronous voltage is $V_{synch} = |V|\sin\phi_s$ and define $I_{synch} = |I_B|\sin\phi_s$. One then has

$$2I_F = V/Z_0 + I_{synch} + V/R_{sh}, \tag{4.7}$$

where we now have real numbers. The power needed to run the cavity is

$$P = \frac{1}{2}I_F^2 Z_0 = \frac{1}{8}Z_0\left(V/Z_0 + I_{synch} + V/R_{sh}\right)^2. \tag{4.8}$$

Minimizing (4.8) with respect to Z_0 minimizes the power consumption. Not surprisingly one gets

$$P = \frac{1}{2}VI_{synch} + \frac{V^2}{2R}, \tag{4.9}$$

but with the caveat that

$$\frac{1}{Z_0} = \frac{I_{synch}}{V} + \frac{1}{R}. \tag{4.10}$$

If we keep VI_{synch} fixed and vary the total voltage with beam current, Equation 4.10 implies that we can keep Z_0 constant. Note that the total power might be larger than necessary in this case since V might be larger than required. For definiteness consider the 20 GeV, 25 MW case. Take a power per cavity of $\sim$ 500 kW so we have 50 cavities. The radiative energy loss per turn implies a synchronous voltage of 53 MV and with $\tan\phi_s = 2$ we need 1.2 MV per cavity. With $R = 7$ MΩ we have $Z_0 = 1$ MΩ and a cavity power of 600 kW while for $1/R = 0$ we get $Z_0 = 1.3$ MΩ and 500 kW. For 25 cavities the superconducting case requires 1 MW per cavity while the warm case needs 1.4 MW per cavity.

4.5 Parasitic beam-beam interactions

With a large number of bunches the effect of parasitic beam-beam interactions has to be taken into account. Under the constraint of constant current (and constant synchrotron radiation power) it is only possible to increase the number of bunches if the bunch intensities are reduced proportionally. Thus, if the number of bunches in the baseline design, $N = 360$, is increased by an integer factor n, the bunch intensities in both the electron and proton beams must be decreased by that same factor,

$$\begin{aligned} n_p(n) &= \frac{n_{p,0}}{n} \\ n_e(n) &= \frac{n_{e,0}}{n} \end{aligned} \tag{4.11}$$

where the subscript 0 denotes the baseline value for 360 bunches. To gain luminosity in such a scenario the emittances of both beams are reduced by cooling (protons) and stronger focusing in the arcs (electrons), respectively. Assuming that the emittances can be reduced by the same factor of n, then

$$\epsilon(n) = \frac{\epsilon_0}{n} \tag{4.12}$$

where the β-functions at the interaction point are also reduced by the same factor,

$$\beta^*(n) = \frac{\beta_0^*}{n} \tag{4.13}$$

This results in a reduction of the rms beam sizes at the interaction point by the same factor,

$$\sigma^*(n) = \frac{\sigma_0^*}{n}. \tag{4.14}$$

The resulting luminosity is then

$$\begin{aligned} L(n) &= \frac{f_c\, n\, n_e(n) n_p(n)}{4\pi\, \sigma_x^*(n)\sigma_y^*(n)} \\ &= n\, L_0, \end{aligned} \tag{4.15}$$

where L_0 denotes the baseline luminosity for 360 bunches.

With this parameter scaling the head-on beam-beam tune shift parameter is independent of n

$$\xi_{e,p} = \frac{n_{p,e}(n)\, r_0\, \beta_{x,y}^*(n)}{2\pi\, \gamma\, \sigma_{x,y}^*(n)\left(\sigma_x^*(n) + \sigma_y^*(n)\right)} \tag{4.16}$$

The first parasitic collision occurs at a longitudinal distance of

$$\Delta s = \frac{c}{2n\, f_c} \tag{4.17}$$

from the interaction point, where c denotes the speed of light and f_c is the revolution frequency. At this location the horizontal β-function is

$$\beta(\Delta s) = \beta^* \left(1 + \frac{\Delta s^2}{\beta^{*2}}\right) \tag{4.18}$$

With a crossing angle Θ the horizontal separation of the two beams at that location is

$$\Delta x = \Theta \frac{c}{2n\, f_c} \tag{4.19}$$

and therefore the tune shift due to a single parasitic collision is computed as

$$\begin{aligned}\Delta\nu_{\text{para e,p}} &= \frac{n_{p,e}(n)\, r_0\, \beta_0^*(n)\left(1+\Delta s^2/\beta_0^*(n)^2\right)}{2\pi\gamma\Delta x^2} \\ &= \frac{n_{p,e}(n)\, r_0\, \beta_0^*(n)\left(1+\Delta s^2/\beta_0^*(n)^2\right)}{2\pi\gamma\Theta^2\left(\frac{c}{2n\, f_c}\right)^2},\end{aligned} \tag{4.20}$$

which is independent of the bunch scaling parameter n.

Chapter 5

Leading risks

The leading risks of the ring-ring version of eRHIC are **crab cavities**, and **electron cooling of hadrons**. More minor risks include:

1. In-situ copper coating of the RHIC beampipes to allow higher intensities and/or shorter bunches
2. Compact superconducting interaction region quadrupoles
3. Dynamic aperture reduction due to strong interaction region focusing
4. Higher harmonic crab cavities (if any)
5. Faster injection kickers and a new hadron RF system to allow for shorter bunch spacing

Such luminosity upgrade risks are not discussed here, but deserve further study.

5.1 Crab cavities

The crab cavities need to create a 4-bump. A design voltage of $V_\perp = 7.25$ MV at 168 MHz for each of the 4 steerers is adequate. A very preliminary warm cavity design consists of two opposing quarter wave resonators, about 1 m long and 1 m wide, with a height of less than 0.5 m. Two such cavities will generate $V_\perp = 7.25$ MV with 140 kW per cavity, assuming a perfect copper surface. Imperfections in the surface will increase the power required, but improving the shunt impedance with nose-cones will reduce it. A fiducial power of 200 kW per cavity is reasonable.

Higher harmonic cavities may be needed to compensate for the RF curvature and to avoid the associated synchro-betatron resonances that are due to the finite wavelength of the crab cavities, when compared to the relatively long ($\sigma_s = 20$ cm) proton bunches [19]. A definitive evaluation awaits results from the detailed simulation studies that have been initiated.

5.2 Electron cooling of hadrons

Electron cooling of the hadron beam is highly desirable to boost the luminosity at low center-of-mass energies that require proton energies as low as 50 GeV. Without cooling the low energy proton bunch length increases significantly with longitudinal emittance, until the IBS growth times have decreased to reasonable values of several hours. Longer bunches require larger values of β^* to limit the luminosity reduction due to the hourglass effect, as well as due to the RF curvature of the crab cavity waveform.

Electron cooling with bunched electron beams will be used in the Low Energy RHIC electron Cooler (LEReC) in 2018, serving as a proof-of-principle of bunched beam electron cooling. In the interest of cost savings a staged approach could be implemented in eRHIC, gradually increasing the beam energy of the

cooler with successively added RF cavities. This would also ease the learning curve, since cooling times at lower energies are significantly shorter, making tuning and optimizing the electron cooler easier.

Appendix A

RF power reduction

The baseline scenario described in Section 2.1 assumes a linear synchrotron power loss limitation of 10 kW/m in the arcs, which is the current state-of-the-art technical limit. With a total arc length of roughly 2400 m, this corresponds to a required RF power of 24 MW. Assuming a typical klystron efficiency of 60%, the electrical power consumption of the electron RF system alone is about 40 MW, or about five times the current power consumption of the RHIC facility [20]. It is therefore worth considering potential power savings, and the associated luminosity reduction.

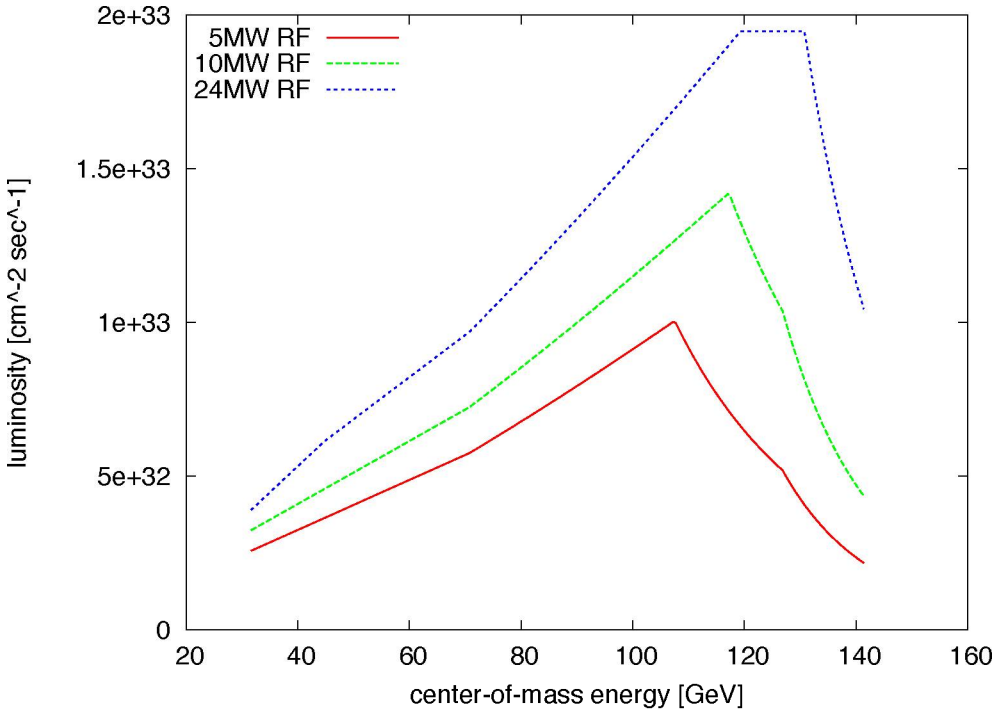

Figure A.1: Head-on luminosity versus center-of-mass energy for three different RF power limits in the electron ring.

In doing so, we assume the same beam parameters and scaling laws as in the baseline design:

- Normalized proton emittance $\epsilon_{n,p} = 2.5$ μm;
- Proton rms bunch length $\sigma_s = 20$ cm (requiring magnetized electron cooling at low energies);

- Electron emittances $\epsilon_{x,e} = 53$ nm, $\epsilon_{y,e} = 9.5$ nm;
- Proton β-functions $\beta^*_{x,p} = 2.16$ m, $\beta^*_{y,p} = 0.27$ m;
- Maximum proton bunch intensity $N_p = 3 \times 10^{11}$;
- Beam-beam scaling with damping decrement as in B-factories: $\xi_e = 1.37\delta^{1/3}$;
- Damping wigglers to increase the damping decrement by increasing the SR power to the RF limit.

Figure A.1 depicts the resulting head-on luminosity curves for three total RF power limits of 5, 10, and 24 MW. As this graph demonstrates, limiting the electron RF power mainly reduces the luminosity at high center-of-mass energies, and as a result the highest luminosity is reached at lower and lower energies the more the RF power is reduced. However, even at a total RF power of only 5 MW a peak luminosity of 1×10^{33} cm^{-2}sec^{-1} is reached at a center-of-mass energy of roughly 100 GeV.

A further reduction of the required RF power, or, conversely, a luminosity increase for a given RF power, can be achieved by means of magnetized electron cooling. Reducing the transverse proton emittances as well as the proton bunch length by a factor of two, to $\epsilon_{n,p} = 1.25$ μm and $\sigma_{s,p} = 10$ cm, respectively, and in turn reducing the electron β-functions at the interaction point by that same factor of two to $\beta_{x,e} = 0.19$ m and $\beta_{y,e} = 0.135$ m yields the same luminosities at half the RF power as in the case without cooling, as shown in Figure A.2.

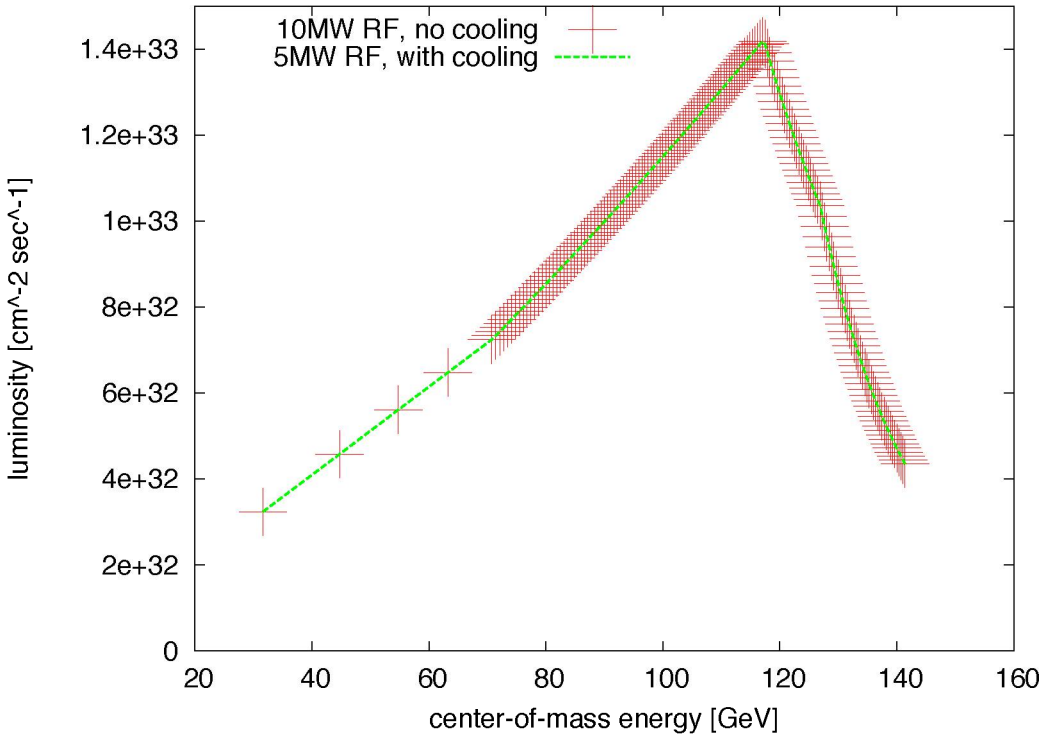

Figure A.2: Head-on luminosity versus center-of-mass energy for an RF power limit of 10 MW without cooling, and for an RF power limit of 5 MW with electron cooling.

The reduced electron beam β-functions in the cooling scenario require some modifications to the interaction region. The magnet apertures of the electron low-β triplet have to be increased by roughly 40 percent to accommodate the increased beam size while keeping the same gradient as in the baseline design. Assuming that the resulting increased peak field of these quadrupoles requires additional space for the superconducting coils the separation of the electron beam and the neutron cone has to be increased as well.

This can be accomplished by an increased crossing angle of 20 mrad (vs. 15 mrad in the baseline design). This necessitates a higher crab cavity voltage of 10 kV to approximately restore head-on collisions. Due to the reduced proton bunch length of 10 cm this restores 95 percent of the head-on short bunch luminosity, assuming the same 168 MHz crab cavity frequency as in the baseline design. Figure A.3 depicts the modified interaction region.

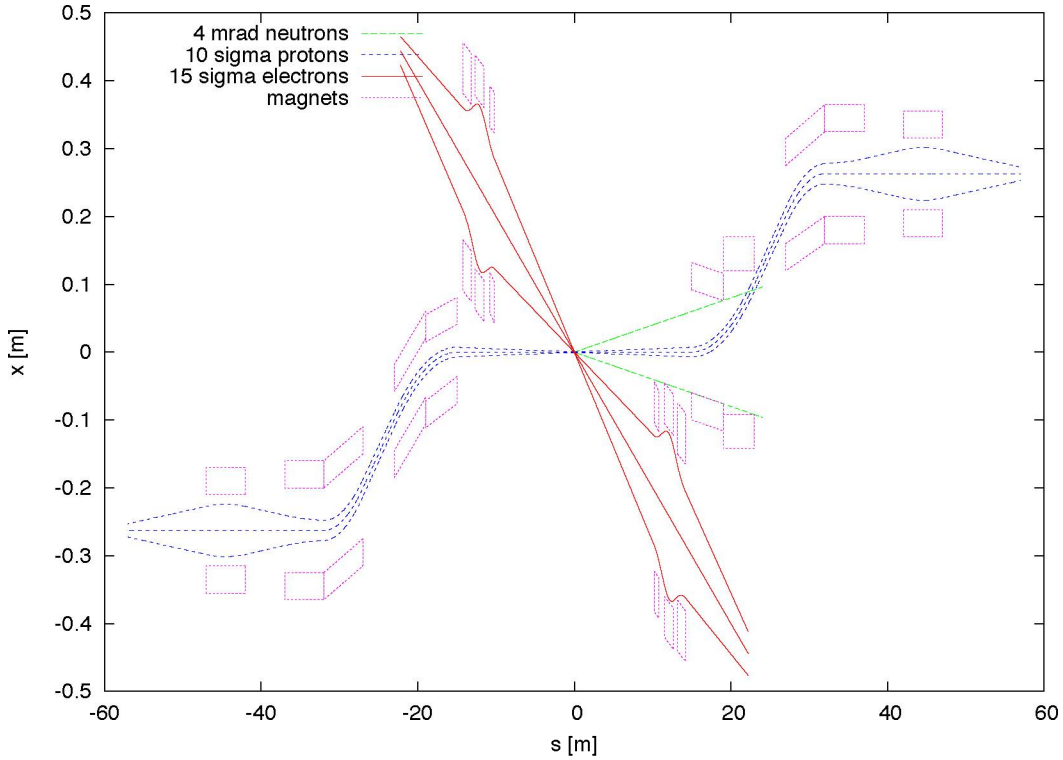

Figure A.3: Top view of the modified interaction region in the electron cooling scenario.

Appendix B

A comparison of FODO and Triple Achromat Lattice electron optics

Two options for the arcs – FODO cell and the Triplet Achromat Lattice (TAL) cell are presented here [12, 13]. Their corresponding advantages and disadvantages are discussed.

These arcs are presented with a packing factor that results in a dipole radius of curvature of about 300 m. One could consider reducing the length of the arc cells (needing more cells per arc). Thus, the packing factor is reduced requiring a smaller dipole bending radius to fit in the existing tunnel. The result is a compromise between increased electron radiation and reduced un-normalized emittance.

FODO cell optics

A FODO cell is proposed that is the same length as a RHIC cell averaged between the inner and outer cells. The dipoles were increased in length and all drift spaces are reduced to 1 m length (this may need to be modified depending on the additional sextupole, orbit correctors, etc that will need to be added), keeping the total cell length unchanged. The increased bending radius, 300.612 m, in the dipoles reduces the electron's radiative energy. A full arc consists of 11 FODO cells and a full ring consists of 6 arcs. The cell length is 29.6221 m.

Three FODO cells are shown in Figs. B.1, B.2 and B.3 for the three operating conditions 5 GeV, 10 GeV and 20 GeV respectively. The vertical phase advance is fixed to $\Phi_y = 90.0^\circ$ in these cases, which is currently a free parameter. The large horizontal phase advance at 20 GeV to get a low enough un-normalized emittance to meet the requirements is a concern. The large variation of the horizontal phase advance – over the different operating conditions – increases the difficulty of designing the matching section to the interaction regions. Wigglers can improve this situation by increasing the un-normalized emittance at the lower energies, 5 GeV and 10 GeV. Table B.1 shows the FODO cell properties.

Triplet Achromat Lattice optics

A low emittance cell used in electron machines is called the Triplet Achromat Lattice (TAL) cell [12]. The length is chosen so that 12 cells fits into the Arc. The cell length is 27.1536 m. The bending radius is 293.083 m, slightly smaller than the FODO cells described above. The drift spaces are 1 m in length. A full arc consists of 12 TAL cells and a full ring consists of 6 Arcs.

Three TAL cells are shown in Figs. B.4, B.5 and B.6 for the three operating conditions 5 GeV, 10 GeV and 20 GeV respectively. The vertical phase advance is fixed to $\Phi_y = 90.0^\circ$ in these cases, which is currently a free parameter. The horizontal phase advance at 20 GeV was chosen to get the required un-normalized emittance. There is some room to play if this requirement changes in the future. As with the FODO cells, the large variation of the horizontal phase advance – over the different operating conditions – increases the difficulty of designing the matching section to the interaction regions. Wigglers can improve

Property	5 GeV	10 GeV	20 GeV
$B\rho$ $[T/m]$	16.6782	33.3564	66.7128
Φ_x $[^\circ]$	35.0	61.5	123.6
Φ_y $[^\circ]$	90.0	90.0	90.0
I_1 $[m]$	0.518391	0.172302	0.0508848
I_2 $[m^{-1}]$	2.58965×10^{-4}	2.5896×10^{-4}	2.58965×10^{-4}
I_3 $[m^{-2}]$	8.61457×10^{-7}	8.61457×10^{-7}	8.61457×10^{-7}
I_4 $[m^{-1}]$	5.73646×10^{-6}	1.90668×10^{-6}	5.63085×10^{-7}
I_5 $[m^{-1}]$	7.31898×10^{-7}	1.3911×10^{-7}	2.3346×10^{-8}
$\langle H \rangle$ $[m]$	0.671206	0.127574	0.0214101
ϵ_{eUH} $[nm]$	106.037	79.4153	53.0342
U_0 $[KeV]$	2.2787	36.4604	583.367
J_x	0.977849	0.992637	0.997826
J_E	2.02215	2.00736	2.00217
D	0.0221515	0.00736268	0.00217437
σ_E/E	2.457×10^{-4}	4.931×10^{-4}	9.876×10^{-4}
ξ_x	-0.20505	-0.22977	-0.53628
ξ_y	-0.24439	-0.27668	-0.3626
G_D $[T/m]$	-1.36084	-2.82503	-6.10867
G_F $[T/m]$	0.94026	2.33268	7.24426

Table B.1: The properties of the FODO cells at each of the three working conditions.

this situation by increasing the un-normalized emittance at the lower energies, 5 GeV and 10 GeV. The needed sextupoles for the TAL cells are expected to be larger than the FODO cells, which will impact the dynamic aperture of the ring. Table B.2 shows the TAL cell properties.

Property	5 GeV	10 GeV	20 GeV
$B\rho$ $[T/m]$	16.6782	33.3564	66.7128
Φ_x $[^\circ]$	31.7	54.9	98.3
Φ_y $[^\circ]$	90.0	90.0	90.0
I_1 $[m]$	0.461048	0.151172	0.045274
I_2 $[m^{-1}]$	2.43483×10^{-4}	2.43483×10^{-4}	2.43483×10^{-4}
I_3 $[m^{-2}]$	8.30766×10^{-7}	8.30766×10^{-7}	8.30766×10^{-7}
I_4 $[m^{-1}]$	5.36742×10^{-6}	1.75991×10^{-6}	5.2707×10^{-7}
I_5 $[m^{-1}]$	6.92279×10^{-7}	1.31047×10^{-7}	2.19023×10^{-8}
$\langle H \rangle$ $[m]$	0.641837	0.121499	0.0203064
ϵ_{eUH} $[nm]$	106.662	79.5588	52.9176
U_0 $[KeV]$	2.14254	34.2807	548.492
J_x	0.977956	0.992772	0.997835
J_E	2.02204	2.00723	2.00216
D	0.0220443	0.00722806	0.00216471
σ_E/E	2.488×10^{-4}	4.995×10^{-4}	0.00100017
ξ_x	-0.17182	-0.17359	-0.26005
ξ_y	-0.27111	-0.30841	-0.42034
G_D $[T/m]$	-3.83506	-8.4929	-20.8763
G_F $[T/m]$	3.25482	7.6762	21.3163

Table B.2: The properties of the Triplet Achromat Lattice cells at each of the three working conditions.

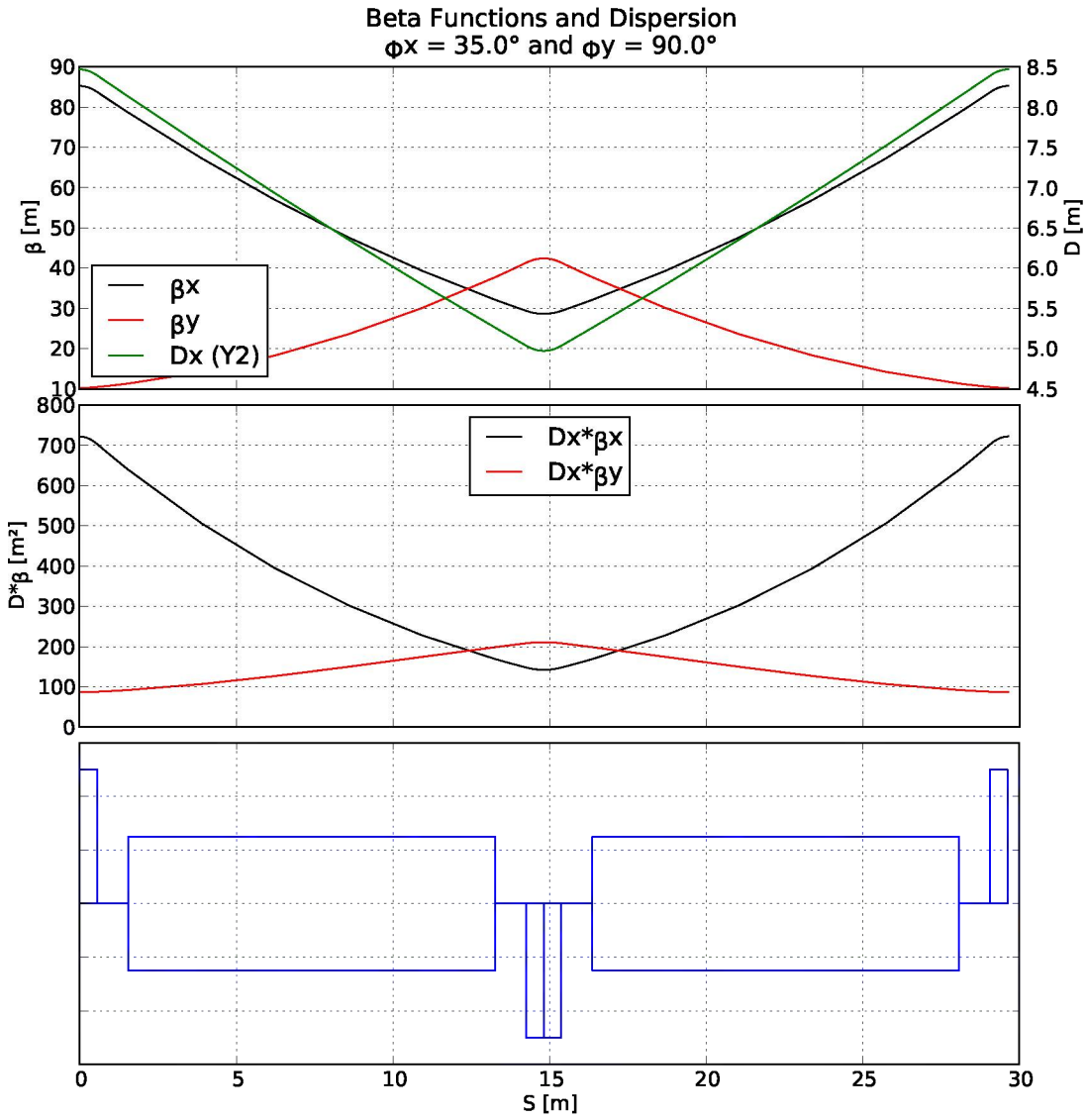

Figure B.1: This shows the FODO cell with $\Phi_x = 35.0^\circ$ and $\Phi_y = 90.0^\circ$. The un-normalized emittance is 106 nm. The top plot shows the Twiss parameters, the middle plot is of the dispersion*beta-function to suggest the best place for the sextupoles and the bottom plot is the schematic of the magnets.

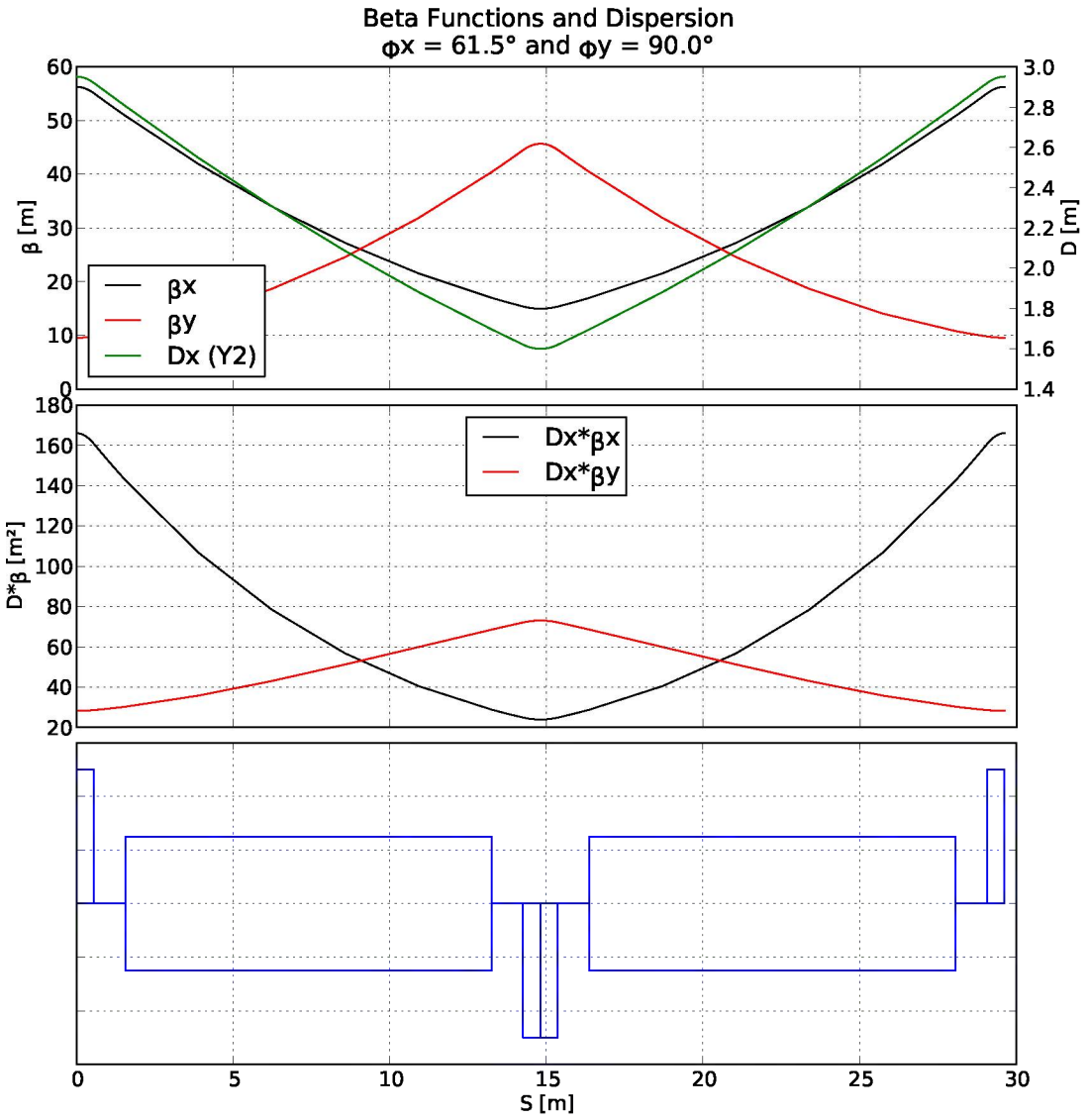

Figure B.2: This shows the FODO cell with $\Phi_x = 61.5^\circ$ and $\Phi_y = 90.0^\circ$. The un-normalized emittance is 79.4 nm. The top plot shows the Twiss parameters, the middle plot is of the dispersion*beta-function to suggest the best place for the sextupoles and the bottom plot is the schematic of the magnets.

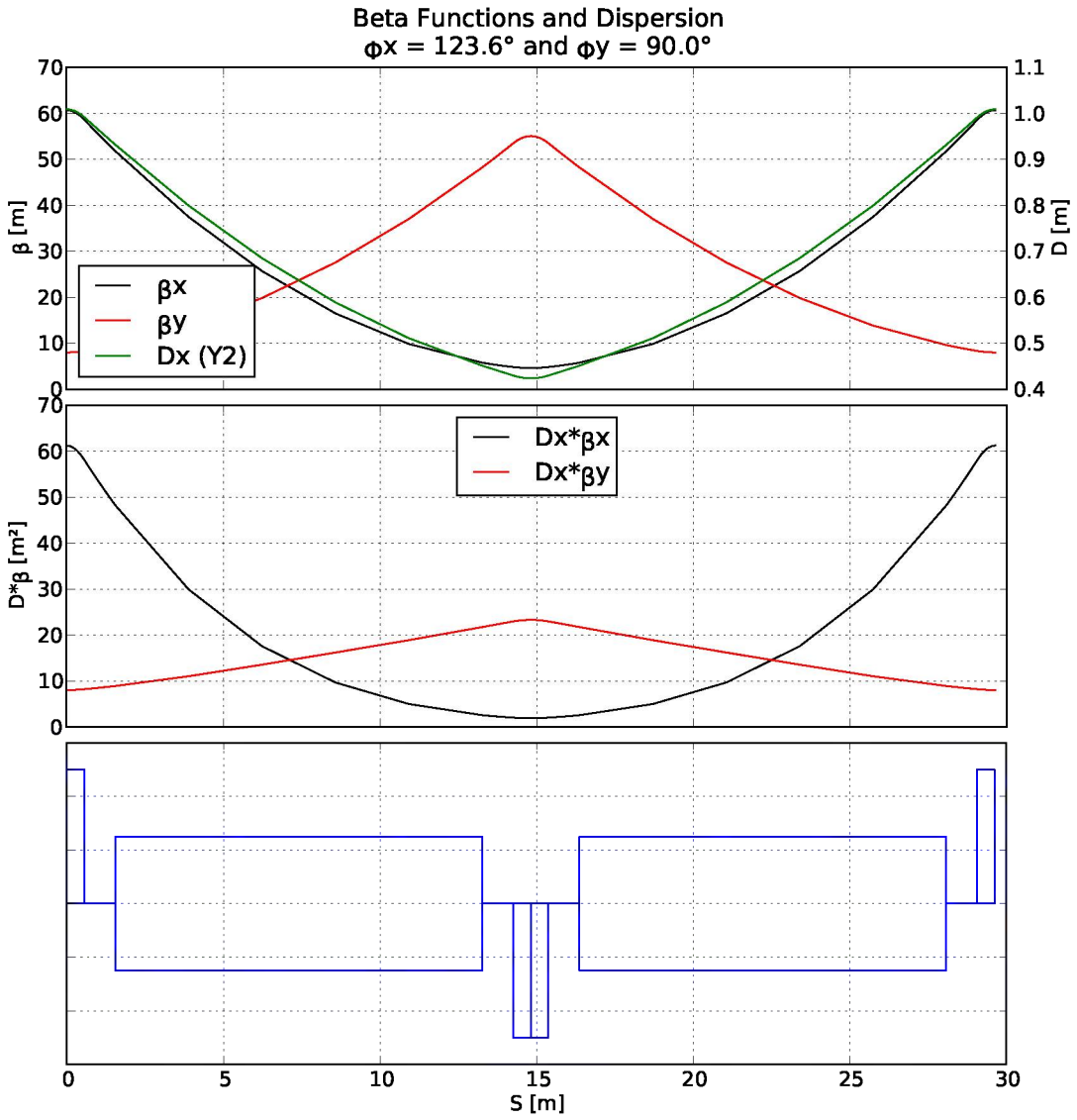

Figure B.3: This shows the FODO cell with $\Phi_x = 123.6^\circ$ and $\Phi_y = 90.0^\circ$. The un-normalized emittance is 53 nm. The top plot shows the Twiss parameters, the middle plot is of the dispersion*beta-function to suggest the best place for the sextupoles and the bottom plot is the schematic of the magnets.

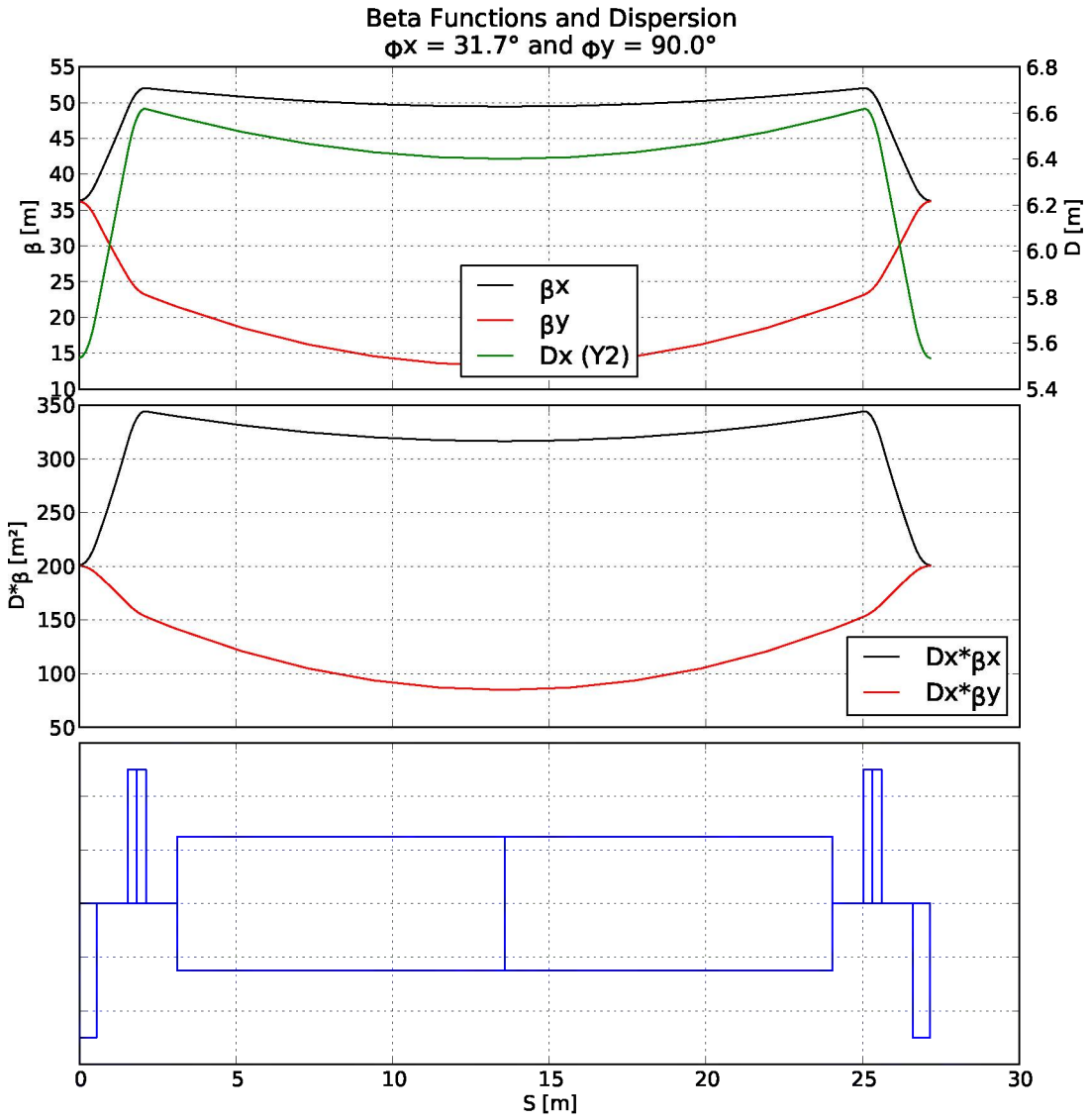

Figure B.4: This shows the TAL cell with $\Phi_x = 31.7^\circ$ and $\Phi_y = 90.0^\circ$. The un-normalized emittance is 106.7 nm. The top plot shows the Twiss parameters, the middle plot is of the dispersion*beta-function to suggest the best place for the sextupoles and the bottom plot is the schematic of the magnets.

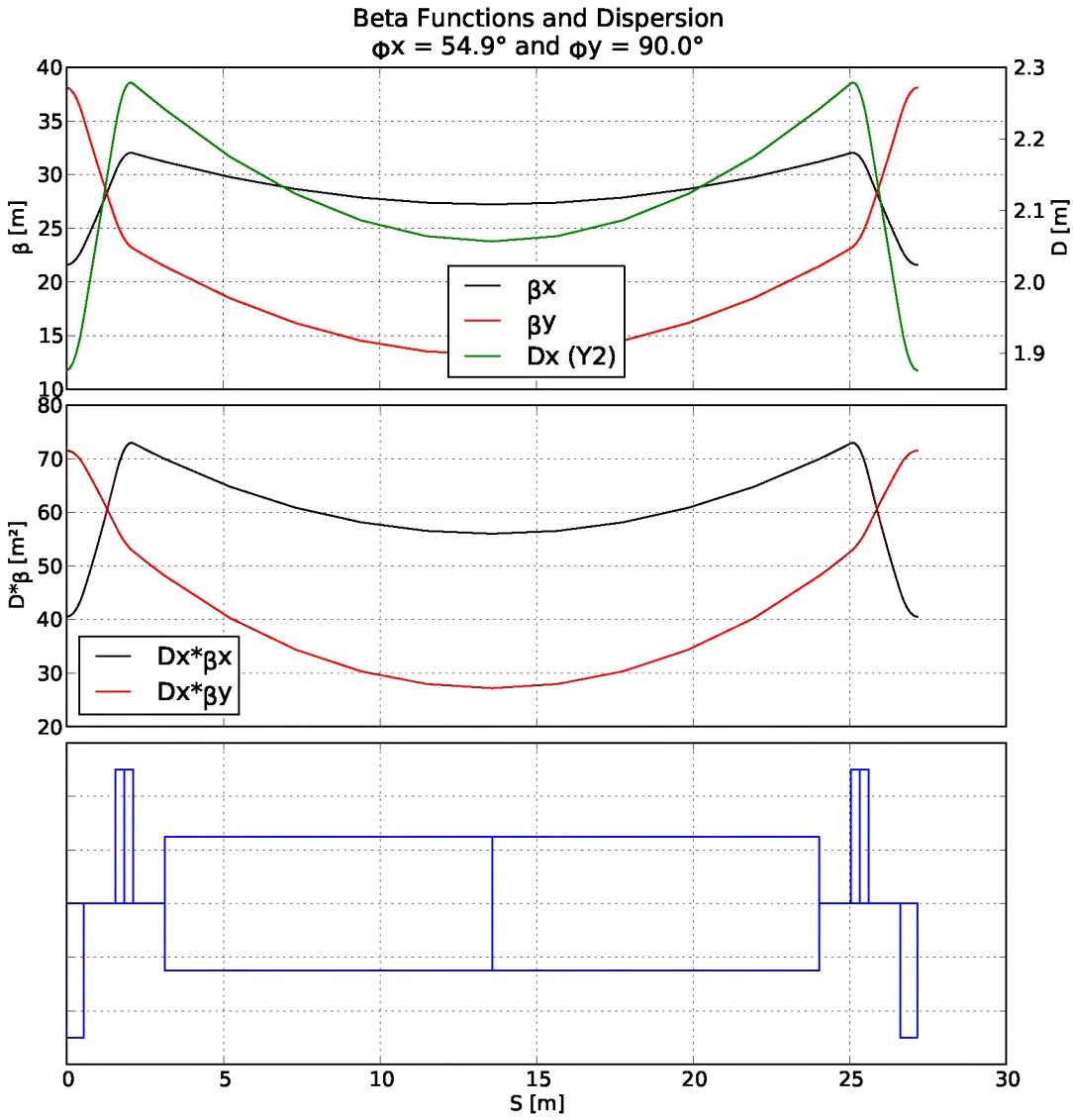

Figure B.5: This shows the TAL cell with $\Phi_x = 54.9^\circ$ and $\Phi_y = 90.0^\circ$. The un-normalized emittance is 79.6 nm. The top plot shows the Twiss parameters, the middle plot is of the dispersion*beta-function to suggest the best place for the sextupoles and the bottom plot is the schematic of the magnets.

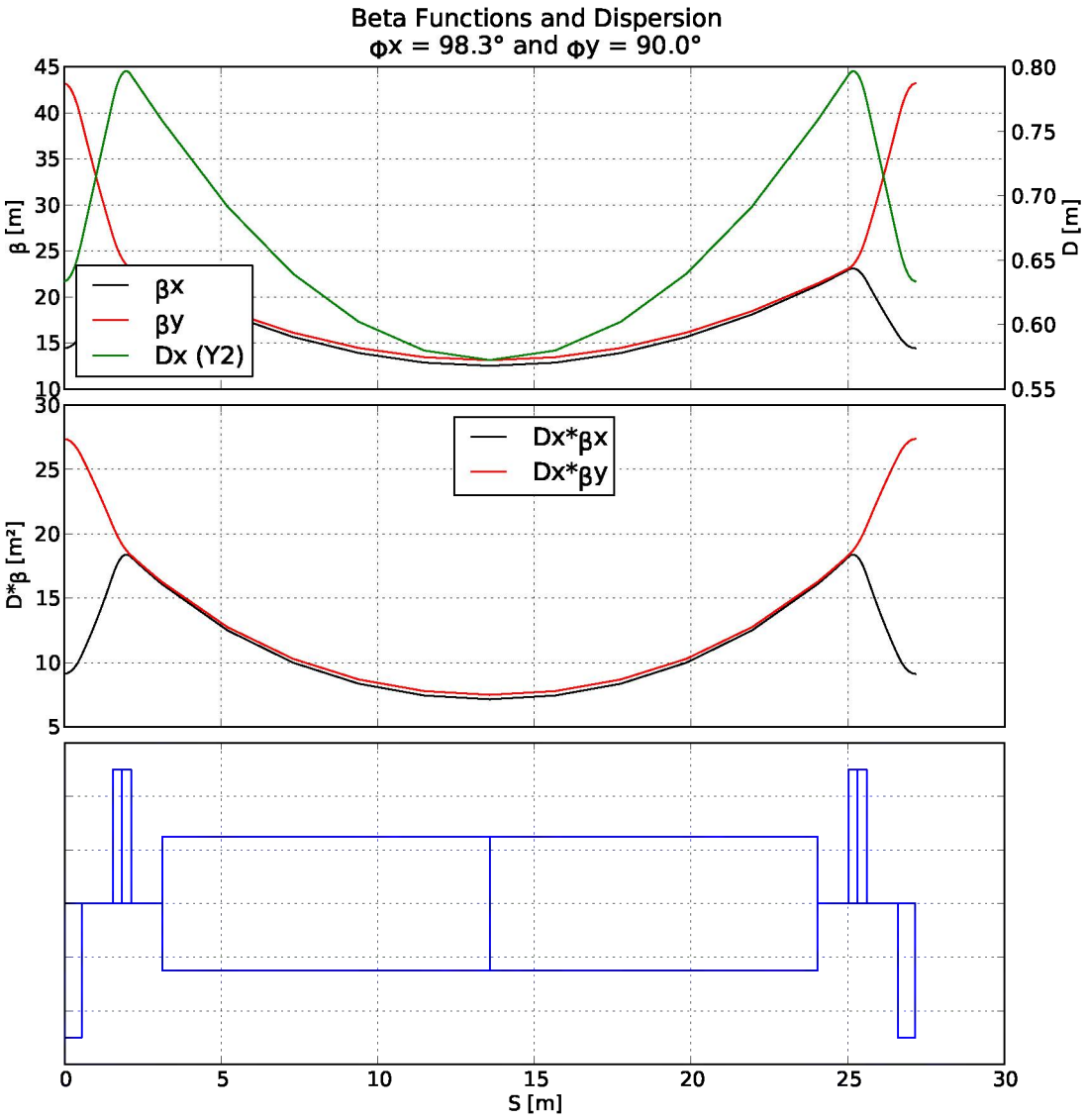

Figure B.6: This shows the FODO cell with $\Phi_x = 98.3^\circ$ and $\Phi_y = 90.0^\circ$. The un-normalized emittance is 52.9 nm. The top plot shows the Twiss parameters, the middle plot is of the dispersion*beta-function to suggest the best place for the sextupoles and the bottom plot is the schematic of the magnets.

Bibliography

[1] I. Ben-Zvi, J. Kewisch, J. Murphy, and S. Peggs, *Accelerator Physics Issues in eRHIC*, NIMA 463 **94** (2001).

[2] M. Farkhondeh and V. Ptitsyn (eds.), *eRHIC Zeroth-Order Design Report*, C-A/AP/142 (2004).

[3] Y. Zhang, *An alternate ring-ring design for eRHIC*, arXiv:1502.07721 (JLAB, 2015).

[4] E. Aschenauer et al., *IR Design Requirements*, eRHIC wiki.
https://wiki.bnl.gov/eic/index.php/IR_Design_Requirements

[5] Y. Funakoshi for the KEKB commissioning group, *Beam-beam effects observed at the KEKB*, ICFA Proceedings, Factories 2001, (2001);
T. Ieiri et al., *Measurement of coherent beam-beam tune shift under crabbing collision at KEKB*, PRSTAB 12 064401 (2009).

[6] M. Sands, *The physics of electron storage rings*, SLAC-121 (SLAC, 1970).

[7] I. Ben-Zvi et al (BNL) and I. Bazarov et al. (Cornell University), *A white paper: The Cornell-BNL FFAC ERL Test Accelerator*, internal communication (BNL and Cornell, December 2014).

[8] J. Seeman, *Top Up Injection at PEP-II and Applications to a Circular e+e- Higgs Factory*, SAT4A1 Proceedings HF2014 (Beijing, China 2014).

[9] A. Accardi et al., *Electron Ion Collider: The Next QCD Frontier - Understanding the glue that binds us all* arXiv:1212.1701 (2014).

[10] E. Aschenauer et al., *RHIC Design Study: An Electron-Ion Collider at BNL*, (BNL, 2014).

[11] U. Schnekloth, *The HERA ep Interaction Regions - Learned Lessons*,
https://wiki.bnl.gov/eic/upload/InteractionRegion_Schneekloth.pdf (Hampton University, 2008).

[12] A. Ropert, *Low Emittance Lattices*, CERN 95-06 147-166 (1995).

[13] S.Y. Lee, *Accelerator Physics*, World Scientific (1999).

[14] Ya.S. Derbenev and A.M. Kondratenko, Sov. Phys. IJETP **35** 2306A (1972).

[15] S.R. Mane, Yu. M. Shatunov and K. Yokoya, *Report on Progress in Physics* **68** 1997 (2005).

[16] R. Assmann et al., Proceedings of EPAC, London, p.932 (1994).

[17] D.P. Barber, et al., Phys. Lett. **3434B** 436 (1995).

[18] T. Zwart, et al., Proceedings of PAC, Chicago, p.3597 (2001).

[19] C. Montag, NIMA 582, 390-394 (2007).

[20] K.A. Drees, Private communication (2015).